NAVAL POSTGRADUATE SCHOOL

MONTEREY, CALIFORNIA

THESIS

GENERATION OF SQUEEZED LIGHT FOR USE WITH ATOM INTERFEROMETERS

by

Renata da Cruz Araújo Vieira

December 2020

Thesis Advisor: Francesco A. Narducci
Second Reader: Jihane Mimih

THIS PAGE INTENTIONALLY LEFT BLANK

REPORT DOCUMENTATION PAGE			*Form Approved OMB No. 0704-0188*

1. AGENCY USE ONLY *(Leave blank)*	**2. REPORT DATE** December 2020	**3. REPORT TYPE AND DATES COVERED** Master's thesis

4. TITLE AND SUBTITLE GENERATION OF SQUEEZED LIGHT FOR USE WITH ATOM INTERFEROMETERS	**5. FUNDING NUMBERS** RP282
6. AUTHOR(S) Renata da Cruz Araújo Vieira	
7. PERFORMING ORGANIZATION NAME(S) AND ADDRESS(ES) Naval Postgraduate School Monterey, CA 93943-5000	**8. PERFORMING ORGANIZATION REPORT NUMBER**
9. SPONSORING / MONITORING AGENCY NAME(S) AND ADDRESS(ES) Washington, D.C., 20301	**10. SPONSORING / MONITORING AGENCY REPORT NUMBER**

11. SUPPLEMENTARY NOTES The views expressed in this thesis are those of the author and do not reflect the official policy or position of the Department of Defense or the U.S. Government.

12a. DISTRIBUTION / AVAILABILITY STATEMENT Approved for public release. Distribution is unlimited.	**12b. DISTRIBUTION CODE** A

13. ABSTRACT (maximum 200 words)

Atom interferometers possess great potential as sensitive and stable acceleration and rotation sensors. Currently, the DoD is interested in leveraging atom interferometry research to improve inertial sensors and develop portable, compact devices based on atom interferometers with strategic-grade performance. Typical atom interferometers measure the acceleration or rotation signal with an on-resonance detection laser field, but these laser fields have inherent noise that degrades the signal-to-noise ratio. The laser noise in one quadrature of the field can be reduced below the so-called shot noise limit at the expense of the other quadrature. Fields with this property are called "squeezed fields." Although lowering the noise in one quadrature increases noise in the other quadrature (due to Heisenberg's uncertainty principle), the noise in the other quadrature can be made irrelevant by designing a detection scheme that does not use that quadrature. By reducing light-source noise, atom interferometer measurement precision can be increased. This thesis aims to establish the groundwork for creating squeezed light to be used for the detection of atoms in the ground or excited state of the NPS Atom Interferometry Laboratory atom interferometer.

14. SUBJECT TERMS atom interferometry, laser noise, quantum noise	**15. NUMBER OF PAGES** 95
	16. PRICE CODE

17. SECURITY CLASSIFICATION OF REPORT	**18. SECURITY CLASSIFICATION OF THIS PAGE**	**19. SECURITY CLASSIFICATION OF ABSTRACT**	**20. LIMITATION OF ABSTRACT**
Unclassified	Unclassified	Unclassified	UU

NSN 7540-01-280-5500 Standard Form 298 (Rev. 2-89) Prescribed by ANSI Std. 239-18

THIS PAGE INTENTIONALLY LEFT BLANK

Approved for public release. Distribution is unlimited.

GENERATION OF SQUEEZED LIGHT FOR USE WITH ATOM INTERFEROMETERS

Renata da Cruz Araújo Vieira
Lieutenant, United States Navy
BS, Universidade Federal do Espirito Santo, 1999

Submitted in partial fulfillment of the
requirements for the degree of

MASTER OF SCIENCE IN APPLIED PHYSICS

from the

NAVAL POSTGRADUATE SCHOOL
December 2020

Approved by: Francesco A. Narducci
Advisor

Jihane Mimih
Second Reader

Kevin B. Smith
Chair, Department of Physics

THIS PAGE INTENTIONALLY LEFT BLANK

ABSTRACT

Atom interferometers possess great potential as sensitive and stable acceleration and rotation sensors. Currently, the Department of Defense (DoD) is interested in leveraging atom interferometry research to improve inertial sensors and develop portable, compact devices based on atom interferometers with strategic-grade performance. Typical atom interferometers measure the acceleration or rotation signal with an on-resonance detection laser field, but these laser fields have inherent noise that degrades the signal-to-noise ratio. The laser noise in one quadrature of the field can be reduced below the so-called shot noise limit at the expense of the other quadrature. Fields with this property are called "squeezed fields." Although lowering the noise in one quadrature increases noise in the other quadrature (due to Heisenberg's uncertainty principle), the noise in the other quadrature can be made irrelevant by designing a detection scheme that does not use that quadrature. By reducing light-source noise, atom interferometer measurement precision can be increased. This thesis aims to establish the groundwork for creating squeezed light to be used for the detection of atoms in the ground or excited state of the NPS Atom Interferometry Laboratory atom interferometer.

THIS PAGE INTENTIONALLY LEFT BLANK

Table of Contents

List of Figures

List of Tables

THIS PAGE INTENTIONALLY LEFT BLANK

List of Acronyms and Abbreviations

ARW	angle random walk
AIL	atom interferometry laboratory
APD	avalanche photodetector
DoD	Department of Defense
FWM	four-wave mixing
FWHM	full width at half medium
GPS	global positioning system
INS	inertial navigation system
LRG	laser ring gyro
NPS	Naval Postgraduate School
NEP	noise equivalent power
SNR	signal-to-noise ratio
USN	U.S. Navy

THIS PAGE INTENTIONALLY LEFT BLANK

Acknowledgments

I thank the U.S. Navy for giving me the opportunity to come to the Naval Postgraduate School to study Applied Physics. It was a real gift to take a break from my career to learn physics at the graduate level and complete this degree. I have a newfound appreciation for the physicists that studying the forces of nature makes our lives better.

I am very fortunate to have been advised by Dr. Frank Narducci. He was always available to teach, to repeat what he taught when necessary, to support and encourage me as I dipped my toes into the intriguing waters of quantum mechanics. I appreciate his knowledge, diligence, good-humor, and especially the patience he showed to me.

I would also like to thank Dr. Jeff Lee for building several electronic devices for my experiments, explaining how they worked, and helping me with their installation. Also, for assisting me with equipment troubleshooting that, in times of COVID-19, took hours and lots of patience to get done remotely.

I am grateful for all faculty members, staff, and students of the NPS Department of Physics who were part of my journey and helped me one way or another to get to the end.

Finally, I would like to thank my mom, Maria Célia, my dad, José Raimundo, and my dear husband, Leland, for their love and support.

THIS PAGE INTENTIONALLY LEFT BLANK

CHAPTER 1:
Introduction

1.1 Background

Accurate ship's positioning has always been paramount for navigation. This accuracy ensures that ships follow the planned route, and secondly, it provides safe navigation around hazardous areas and maritime traffic (piloting). The first navigators looked to the stars in the skies for orientation. In the 17th century, sailors measured the speed over water by a simple yet creative technique. A lead-weighted pie-shaped log with a coiled rope around it was tossed to the water. The other side of the rope remained onboard the vessel. The log floated in the water and remained stationary as the sailors allowed the free release of the rope as the vessel moved. An interval of time was measured (with a sandglass), and the log was pulled back on board. The number of knots in the released rope was then counted, and then the speed of the ship could be measured in knots. A knot is equivalent to one nautical mile per hour [1].

The combination of the ability to take position fixes (measuring angles to reference points) and measurement time (making it possible to measure speed over water) results in the dead reckoning process. This process starts by accessing the vessel's initial position, determining the distance traveled in a known direction from the initial position during a period of time, and subsequently continuing to add the displacement vectors every time the ship changes direction [2]. In the 18th century, the invention of the maritime watch by the English carpenter John Harrison enabled the accurate determination of longitude, which was a significant development in onboard navigation [3]. The longitude was determined by keeping two watches onboard the ship: one tracking the time at the shore and one marking the time underway. Every day at sea, the navigator reset the ship's clock when the sun reached the highest point in the sky. Every hour difference between the shore and ship's time was equivalent to 15° of longitude [3].

Dead reckoning navigation, even using better equipment and maps, is still susceptible to errors while estimating set (the effect the tide or wind has on the ship's movement, measured in degrees) and drift (the velocity of the current, measured in knots). The navigational fix can be affected by physical and atmospheric conditions, compromising measurements of distances and angles. An infamous example of a dead reckoning shortfall is the Honda Point disaster off California's coast in 1923. During a naval exercise, 13 of 14 ships either ran aground or collided with each other, resulting in the loss of 23 men [4].

1.2 Current Positioning Techniques

Today, the well-established technology to precisely and accurately determine a ship's position is the satellite-driven global positioning system (GPS). GPS offers unrivaled accuracy for navigation, tracking, and precision targeting. Still, it is heavily relied upon, and as such, any degradation or loss of GPS brings significant risk to the Navy. The risk of a mission-degrading GPS glitch can be natural or man-made. Among the dangers are solar interference, geomagnetic storms, accidental radio interference, system malfunctioning due to lack of necessary satellite maintenance, and, most importantly, the hostile threat of hacking, spoofing, jamming, or physical satellite attacks [5].

Another mature technology in the measurement of ship's movements is onboard inertial navigation system (INS). The basic INS combines at least three gyroscopes for determination of rotation angles with three accelerometers for linear acceleration measurements. With this information, the position can be estimated by a dead-reckoning calculation [6]; however, any small error in angular velocity and acceleration will result in progressively larger errors as these quantities are integrated to calculate position. Furthermore, these sensors are also subject to drift, meaning the sensor output can change even when linear acceleration or rotation rate remained fixed or when the sense is stationary. The position is calculated by integrating the acceleration twice, and the rotation rate is integrated once, further compounding the errors up to quadratically with time [7].

Currently, laser-ring gyrocopes (LRGs) are used for navigation in several military applications, such as submarines, as well in some commercial aircrafts [8]. The LRGs work based on a rotating Sagnac interferometer where the difference in the paths between two overlapping counter-propagating laser beams traversing inside the interferometer results in a fringe

shift proportional to the angular rotation speed Ω [9]. Even though the LRG represented a great advancement in inertial navigation, it still has issues that are being addressed, such as angle random walk (ARW), bias offset error, instability and temperature bias, shock and vibration sensitivity [10].

1.3 Improvements in Current Technology

Anticipating a worst-case scenario of a total loss of GPS, the Navy returned to its roots, teaching the time-honored celestial navigation skill to Quartermaster and Officers [11], [12]. With GPS loss, the ship's position would be determined based on the onboard INS supplemented by celestial navigation efforts. There are issues with this method. First, even if executed correctly, celestial navigation is most effective at night. Second, weapons systems would still be degraded as they rely heavily on GPS.

One way to improve GPS-denied navigation is by exploiting an extremely accurate and highly sensitive sensor that can detect movement [13]. As stated before, the current INS are prone to errors, but if these errors are minimized, then positioning could be improved. Continuous efforts, even in China, are under development to improve inertial sensors for GPS-denied operation [13]. A type of sensor being researched today that has the potential to be more sensitive and accurate than traditional INS is the atomic or quantum sensor in the form of an atom interferometer.

1.4 Status of Research

Atomic sensors and the field of atom interferometry began with the first proof-of-principle experiments almost three decades ago, showing great promise for real-world quantum sensors [14], [15], [16]. In general, interferometers detect rotation or acceleration by analyzing the wave-like behavior of light (in the case of optical interferometers) or the wave-like behavior of atoms (in the case of atom interferometers). In optical interferometry, phase shifts between two different beams of light can be interpreted as a difference in the distance traveled between each of the waves, and this distance traveled is influenced by the motion of the platform that the interferometer is on (for example, the ship could be a platform). Similarly, in an atom interferometer, a phase shift results from path length differences between atomic waves [17]. The advantage of using atomic waves instead of light waves is that

the detectable path length difference, and thus the minimum phase shift, is much smaller. As the minimum detectable phase shift decreases, the sensitivity to changes in rotation or acceleration increases [18].

In the NPS Atomic Interferometry Laboratory (AIL) atom interferometer, a cloud of atoms is initially prepared in the ground state. When a laser pulse interacts with the cloud, the atoms are put in a superposition of having absorbed a photon (excited state) and not having absorbed a photon (ground state). An atom in a superposition state sometimes acts like an atom that remained in the ground state and sometimes like an atom that was excited. For the part of the atom which absorbed a photon and is now in the excited state, it also receives a momentum kick, causing that part of the atom to move. A second pulse then interacts with the cloud, and the two states of the atom switch – the excited shifts to the ground state and vice versa. In this case, both states change travel direction – the atom shifting from the excited to the ground state emits a photon (stimulated emission), which causes a change in the atom's momentum. A third laser pulse causes the two previously split atom populations to recombine. Subjecting the atoms to acceleration or rotation, like on a moving ship, contributes the length of the path traveled by the atoms. Because the distance traveled by each population was different before recombination, a phase shift exists between the two superimposed populations [17].

In this case, the phase shift directly correlates to the difference in atomic population in one state or another. When using the proper techniques, the number of atoms in each state can be determined and correlated with the distance traveled by each wave, thus providing acceleration or rotation measurements. The detection of the atomic states is accomplished by employing the detection of laser induced fluorescence.

An accurate determination of atomic population in each state (excited or ground) is paramount to determining an atom interferometer's fundamental precision. One factor influencing measurement accuracy is the amount of intensity noise in a laser. Reducing the intensity noise allows for more accurate measurements; however, even a laser completely free from technical noise exhibits quantum noise due to the quantum properties of light. Quantum noise is the fundamental noise observed in optical beams, and it results from the quantum fluctuations of the laser beam's intensity due to the finite number of photons in the beam [19]. Reducing the noise level below the quantum noise is prohibited by the laws

of quantum mechanics.

Although the total amount of quantum noise cannot be reduced, quantum noise is the product of the noise from two different quadratures of the laser field. By manipulating the noise in each of these quadratures, the noise in one can be reduced below the quantum noise level (while increasing the noise in the other). When a laser has a property with noise below the quantum noise, it is called "squeezed light" [20]. The detection laser could exploit squeezed light to reduce the noise of the atom interferometer sensor.

The objective of this thesis is to establish the groundwork for creating squeezed light to be used for the detection of atoms in the ground or excited state in an atom interferometer. This work aims to generate a squeezed light beam tailored to match the parameters of the AIL atom interferometer [21].

1.5 Thesis Organization

Chapter 2 of this thesis describes the saturated absorption spectroscopy, which is the method used to establish the laser frequency required to drive atomic transitions that enable the measurement of the population in one state or the other. Chapter 3 explains how measure the quantum noise, which will serve as a baseline for the squeezed light experiments. The rest of the chapter presents the measurement of excess quantum noise from hot vapor, demonstrating that the designed measurement electronics are good enough to use for the squeezing experiments. Chapter 4 introduces the four-wave mixing (FWM) process that will be utilized in future work to create the squeezed beam, and it also describes the preliminary set-up for the squeezed light experiment. Finally, chapter 5 summarizes the findings and provides recommendations for future work.

1.6 Benefits of Study

In contrast with optical, neutron, or electron interferometers, atom interferometry offers distinct advantages. Atom interferometers are more controllable than electron or neutron interferometers (due to the internal atomic structure), better characterized environmental interactions (due to lack of electric charge), better portability, and lower cost. Atomic properties like the mass, magnetic moment and polarization can be selected over ranges of

several orders of magnitude, offering flexible operational parameters [17], [22]. As such, these advantages provide reasons to study and improve upon atom interferometers.

In addition to offering the U.S. Navy (USN) a more accurate INS that is less susceptible to enemy attack, atom interferometers can have a myriad of other applications, including fundamental physics (detecting gravitation waves or measuring the fine-structure constant) [23], in metrology (gravity reference for the Kibble balance), in geophysics (for measuring groundwater), in civil engineering (sinkhole and mineshaft detection), or in mobile platform operations (oil and minerals prospecting) [17].

CHAPTER 2:
Saturated Absorption Spectroscopy

This chapter describes saturated absorption spectroscopy, which is a method used to determine the laser frequency with respect to the resonance frequency required to drive atomic state transitions from the ground state to the excited state. When the laser's frequency coincides with the resonant frequency of atoms, the atoms can undergo the transitions required for a working atom interferometer and the resulting fluorescence can be used on the interferometer's readouts.

2.1 Light and Matter Interaction–Two-Level Atom

Consider a system consisting of a light source (a laser) and a two-level atom ("two-level" in that the atom has two energy levels called the ground and excited states). The atom in the ground level absorbs a photon from the laser beam, causing the atom to transition to the excited state, as shown in Figure 2.1. Once in the excited state, the atom almost instantly decays to its ground state (typically tens of nanoseconds in the case of alkali atoms), emitting a photon at nearly the same frequency previously absorbed. However, this photon does not return to the laser beam; rather, it scatters in a random direction. Consequently, the loss of this photon from the laser beam causes a dip in the laser's transmitted power at the atom's natural resonant frequency. The resonant frequency, ν_0, is determined by ΔE, the difference between atomic energy levels according to $\Delta E = h\nu_0$, where h is the Planck's constant [24].

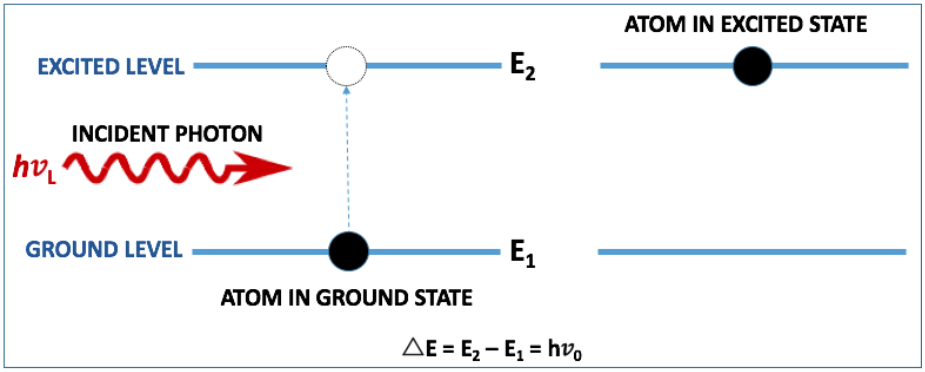

Figure 2.1. Atom in the ground state at rest absorbs a photon and moves to the excited state.

As a consequence of the Heisenberg Uncertainty Principle [25], a downward transition between two states does not result in the emission of a photon at a single wavelength, but instead photons are emitted over a range of frequencies. This principle says there is an uncertainty in the measured energy level difference, ΔE, of an atom as a result of the excited state's intrinsic lifetime, Δt. The relationship describing this uncertainty is given by $\Delta E\, \Delta t \sim \hbar$ [26], where $\hbar$ is the reduced Planck's constant defined as $\hbar = h/(2\pi)$ [27]. As a result, the transition appears as a "spread" of frequencies rather than an infinitely sharp spectral line. The phenomenon described above results in the natural linewidth of the transition [9]. The spectral profile of an emitted photon takes on a Lorentzian shape, as shown in Figure 2.2a. The full width at half maximum (FWHM) is given by the natural linewidth, and is equal to Δt.

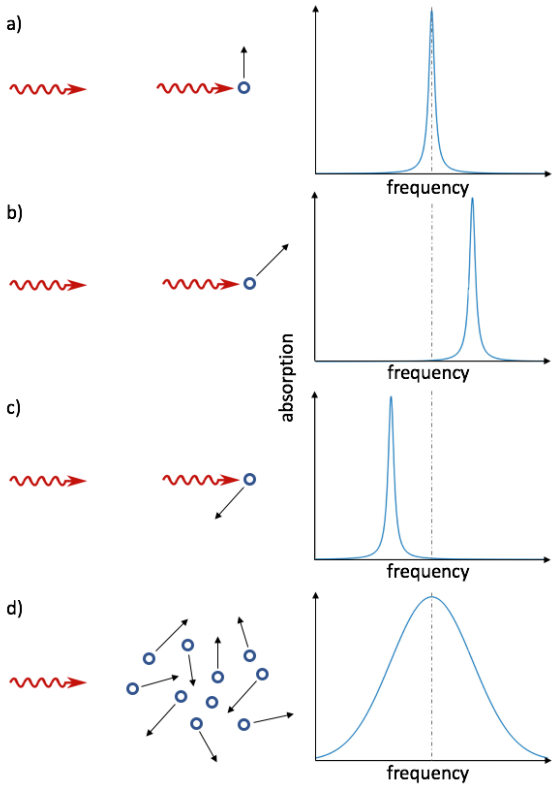

Figure 2.2. Movements of atoms relative to the incoming beam of light shift the frequency of absorption [a, b, c]. A group of atoms with random velocities is expected to follow the Maxwell-Boltzmann distribution [d]. The line shape reflects the sum of contributions of single particles with their distinct velocity vectors. Adapted from [28].

2.2 Doppler-Broadening–Three-Level Atom

Atomic motion results in a broader linewidth due to Doppler shifts. At a temperature above absolute zero, all atoms exhibit random thermal motion, and the amount of motion is a function of the ambient temperature. Atoms traveling toward or away from the laser beam with a velocity v have transition frequencies that differ from those of atoms at rest in the lab frame by the Doppler shift [29].

Figure 2.2b shows an atom moving away from the laser beam. The atom will "see" a lower laser frequency. Thus, the laser frequency will need to be higher to match the atom resonance frequency. Conversely, the opposite happens in Figure 2.2c. The Doppler shift in

the frequency is given by the equation,

$$\nu = \nu_o \left(1 \pm \frac{v}{c}\right), \tag{2.1}$$

where ν_o is the frequency of the atom at rest and c is the speed of light.

In practice, the frequency shifts are shown in the Figure2.2b and c assume a fixed velocity. In a given collection of atoms, observing transition frequencies from individual atoms moving in individual directions is impossible. Instead, we observe the effect of atomic motion averaged over the entire population of atoms. The thermal motion is random, and the distribution of velocities follows the Maxwell-Boltzmann distribution [30]. Because of this velocity distribution, the transition frequencies also have a distribution, resulting in a broadening effect shown in 2.2 d. The broadening of the spectral lines is a result of averaging the entire atom population's individual velocity shifts in the distribution [31]. At room temperature, this broadening effect is typically a factor of 100 times higher than the natural linewidth in the case of Rubidium atoms [32], which is the atom we use in the experiments.

In a two-level hydrogen-like atom, the Doppler broadening effect is not troublesome because there is only one transition. The absorption dip is broadened uniformly around the natural transition frequency due to the Maxwell distribution of velocities which is centered around $v = 0$. In an atom like Rubidium, which is the element used in the AIL atom interferometer, several energy levels exist with different level spacing and transition strengths. The several energy levels result in a Doppler broadened line whose center does not exactly coincide with any transitions. To drive a single energy transition (and the correct one), we must distinguish which exact transitions occur during a laser scan. The Doppler broadening effect causes transitions close to each other to be masked together in a single dip. As a result, it is difficult to identify which transitions occur within the Doppler-broadened absorption dip.

Doppler broadening must be eliminated to determine the frequency that drives explicitly the transitions used in atom interferometry, which occur within the D2 transition of Rubidium-85 (^{85}Rb). One way to eliminate Doppler broadening is by maintaining atoms at absolute zero, but this is unnecessarily difficult. A practical and effective way to mitigate Doppler broadening is by using double-pass saturated absorption spectroscopy.

Rather than using only one laser beam as in single-pass saturated absorption spectroscopy, double-pass saturated absorption spectroscopy utilizes two laser beams. The beams overlap and propagate at the same frequency in opposite directions (counter-propagating). One beam, the pump beam, has higher relative intensity compared to the other beam. When a single laser enters a cell containing a population of atoms above absolute zero in the ground state, the laser excites the atoms and loses photons to absorption. When the laser intensity is high enough to cause the number of atoms in the excited state to be approximately equal to the number in the ground state, the transition is "saturated." In this condition, the atoms in the excited states are equally likely to decay by stimulated emission or spontaneous emission. By scanning the laser over a range of frequencies, we can observe the frequency at which an absorption dip occurs. This measurement is called single-pass spectroscopy, and Doppler broadening limits this type of spectroscopy.

The low intensity beam, called the probe beam, overlaps spatially with the pump beam and so interacts with the same atoms as the pump beam. Due to the Doppler shift, the atom will strongly interact with the pump and the probe at different frequencies. When atoms with relativity low velocities, like the ones moving perpendicular to the laser beams, interact with the pump and the probe at the same frequency as shown in Figure 2.3. When that happens, the pump saturates the atoms. Atoms in the excited state cannot absorb photons from the probe; and so there is an enhancement in the transmission at frequencies close to the natural frequency with no Doppler broadening.

The interaction between the pump and probe beams is shown in Figure 2.3. Only the atoms moving perpendicular to the beams' direction (i.e., not Doppler-shifted) interacts with both beams. As a result, the Doppler broadening effects are mitigated, enabling the identification of the specific laser frequency that drives the desired transition.

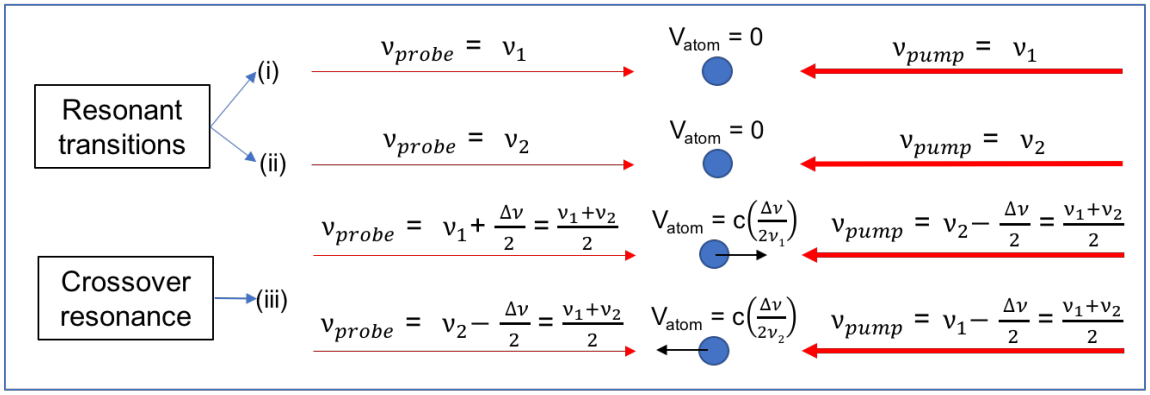

Figure 2.3. Schematics of interactions between overlapping counter-propagating beams of matching frequencies and atoms inside a cell.

Although the double-pass absorption spectroscopy technique eliminates the Doppler broadened masking of transitions, it introduces "artificial transitions" called crossover resonance transitions. Consider a three-level atom with one ground state and two excited states, interacting with counter-propagating beams. The pump beam reduces the probe beam's absorption at the resonant frequencies as just described [31]. Consequently, peaks appears in the probe-transmission spectrum at frequencies ν_1 and ν_2 , as shown in Figure 2.4.

However, consider what happens when the laser is tuned precisely half-way between two transitions. For one velocity class of moving atoms, the Doppler shift will cause the atoms to "see" the pump beam as on-resonance with one transition, e.g., $|g\rangle \rightarrow |e_1\rangle$. That same exact Doppler shift will cause the atoms to "see" the probe Doppler shifted into resonance with the $|g\rangle \rightarrow |e_2\rangle$ transition. Thus, this three-level system "sees" a strong pump which "robs" atoms from the ground state, leaving fewer atoms in the ground state to absorb the probe beam. This effect then results in an increase in the transmission of the probe when the laser is tuned half-way between two transitions. A crossover resonance (iii) is located precisely between the two transition frequencies, (i) and (ii) [31]. This shows that a group

of atoms with velocities that are related to the crossover frequency result in transitions that are driven by the pump and the probe simultaneously, as shown in Figure 2.3 (iii).

Since double-pass spectroscopy relies on the pump and probe interacting with the same atoms, crossover resonances result in artificial peaks that do not represent true transitions. Crossover resonance can be a problem when the transitions are only slightly farther apart than each transition's natural linewidth. As a result, the real absorption peaks could be masked [33]. Fortunately, this is not the case in the transitions we are interested in exploring. The natural linewidth of the Rubidium is about 3 MHz and the level spacing is between 30 MHz and 120 MHz.

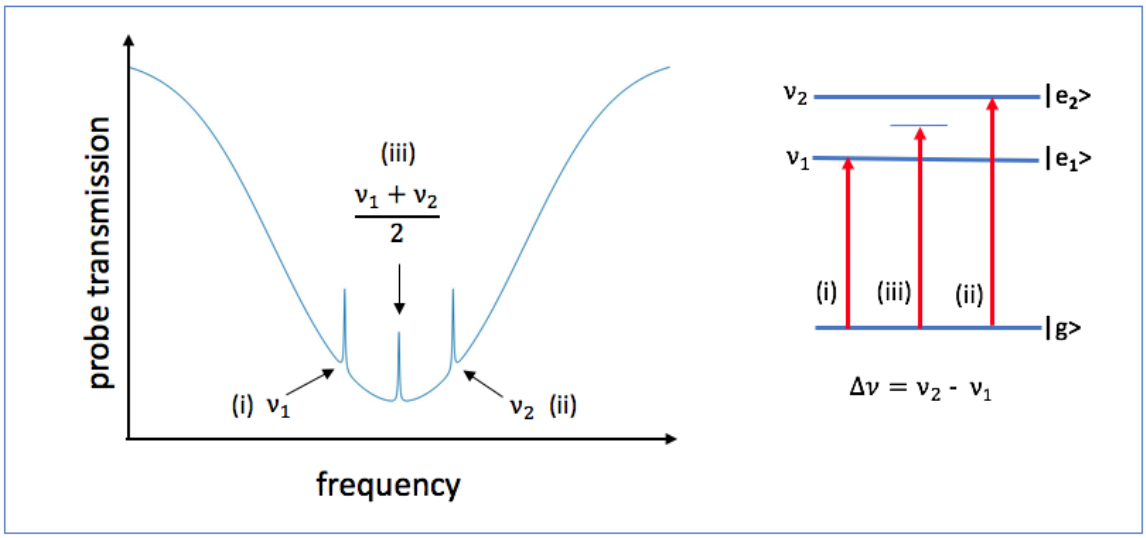

Figure 2.4. Schematic of saturated absorption for atoms with a single ground state and two excited states. Adapted from [34].

2.3 Basic Saturated Absorption Experiment

In this experiment, we will describe the basic saturated absorption experiment. Figure 2.5(a) shows a schematic of the saturated absorption spectroscopy setup, and Figure 2.5(b) is a photograph of the same experimental setup in the laboratory. In this setup, a laser beam passes through an optical isolator, which allows the transmission of light in only one direction, preventing undesirable feedback into the laser cavity. Even at a low level, the feedback could cause increased phase and intensity laser noise, and wavelength instability

[35]. A half-wave plate rotates the linearly polarized laser beam by a controllable amount to form a superposition of horizontal and vertical light. In conjunction with the polarizing beam splitter, adjusting the waveplate angle allows for control of the relative intensities of the now spatially separated vertically and horizontally polarized beam. The horizontally polarized beam is not utilized in the saturation absorption setup, but it will be used in the squeezed light portion of the experiment. The vertically polarized beam passes through the cell containing room temperature Rubidium atomic vapor. The beam saturates the ground to excited state atomic transition and is called a "pump" beam. After the cell, the pump beam passes through a neutral-density filter that reduces the beam intensity. The light passes through a quarter-wave plate, reflected by a mirror, and passed through the quarter-wave plate resulting in the conversion of laser beams' polarization from vertical to horizontal polarization. The now horizontally polarized beam, which has its intensity once more reduced by the neutral density filter, is called the "probe" beam. The probe beam goes through the cell, and a photodiode detector measures its intensity as the laser frequency ν_L is scanned through resonance frequencies.

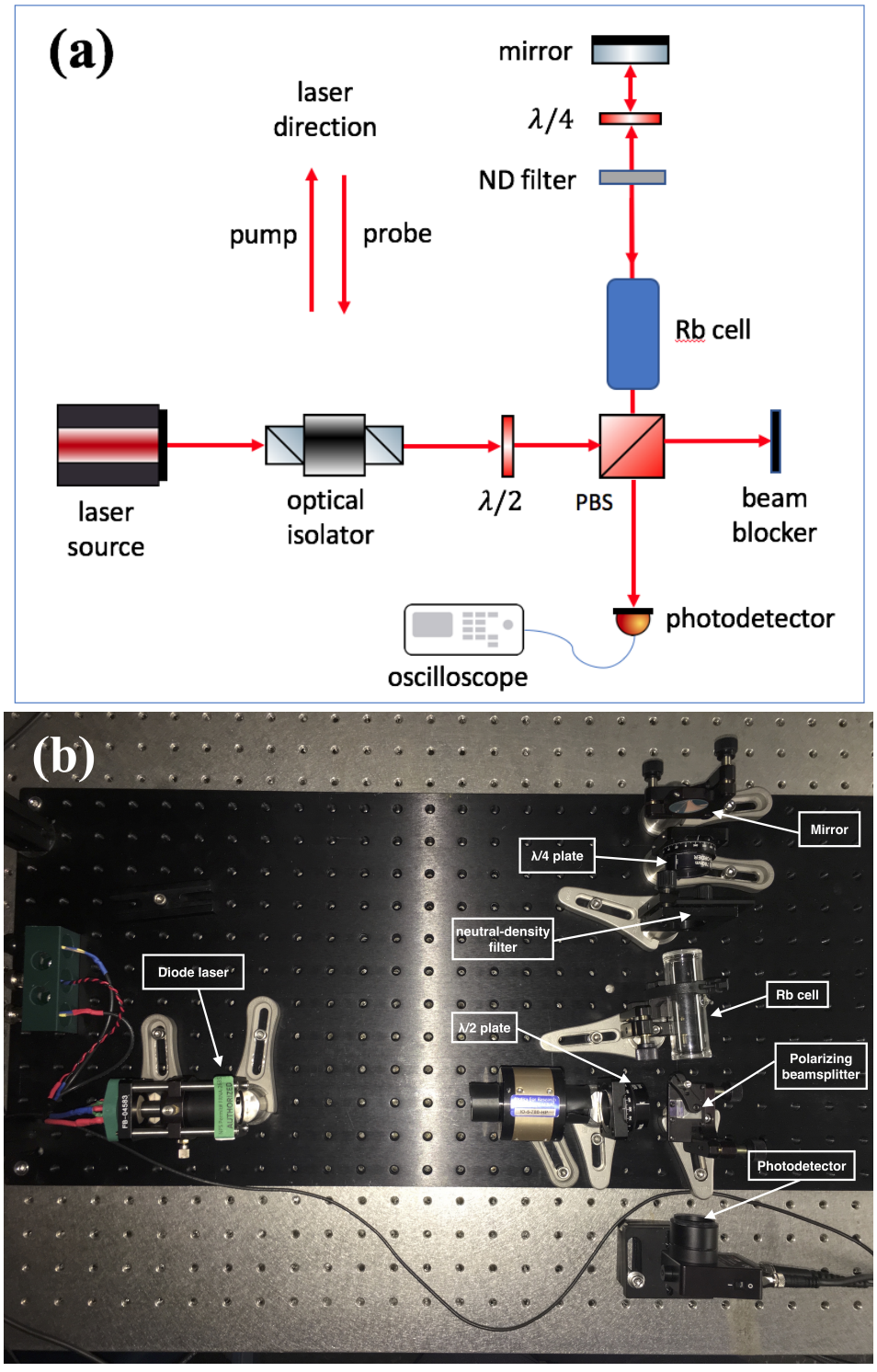

Figure 2.5. Basic saturated absorption experimental schematic (a). Basic saturated absorption experimental setup on optical table (b).

The double-pass absorption spectroscopy experiment shown in Figure 2.5 was accomplished for practice purposes. A more useful, double-pass saturated absorption experiment was built (as shown in Figure 2.7) and will be discussed in subsection 2.3.1.

2.3.1 Saturated Absorption Spectroscopy

The single-pass absorption technique was used to explore the effect of Doppler broadening on the isotopes ^{85}Rb and ^{87}Rb, neither of which are two-level atoms. The upper part of Figure 2.6 shows the energy level diagram of D2 lines of ^{85}Rb and ^{87}Rb isotopes. The D2 line comprises the $5^2S_{1/2}$ to $5^2P_{3/2}$ transition. For ^{85}Rb inside the D2 line, there are hyperfine transitions between ground state $F = 2$ and the excited states $F' = 1, 2, 3$ (labeled "a") and between ground state $F = 3$ and the excited states $F' = 2, 3, 4$ (labeled "b"). For ^{87}Rb inside the D2 line, there are hyperfine transitions between ground state $F = 1$ and the excited states $F' = 0, 1, 2$ (labeled "c") and between ground state $F = 2$ and the excited states $F' = 1, 2, 3$ (labeled "d") [32]. The hyperfine splitting for excited states is small compared to the ground state splitting and, due to Doppler broadening as shown in the lower part of Figure 2.6, cannot be observed in this basic setup. Rather than several hyperfine transitions that would appear as sharp peaks, only four broad peaks (a through d) were observed. This verifies that to observe the hyperfine transitions on the D2 line, which are the transitions used in the AIL interferometer, we must eliminate the Doppler broadening effect.

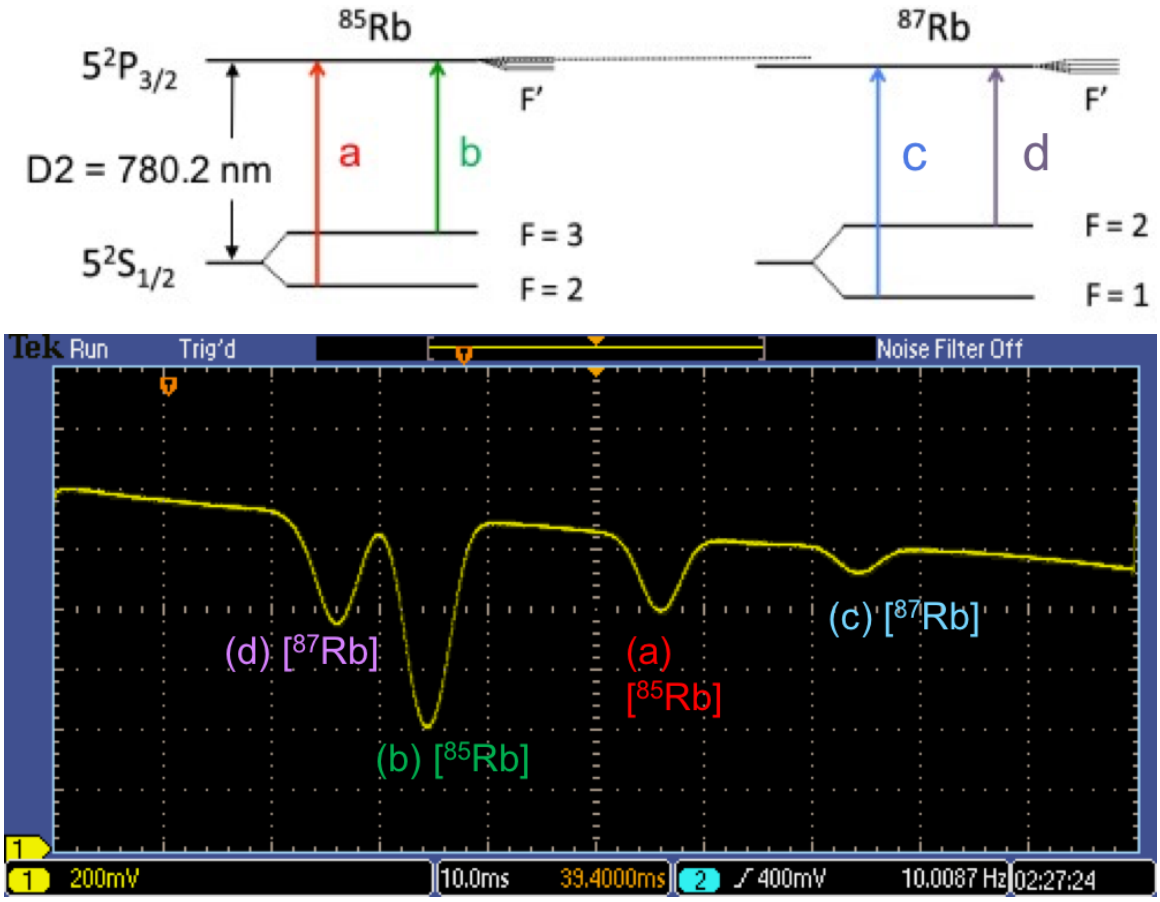

Figure 2.6. Energy level diagram of D2 lines of ^{85}Rb and ^{87}Rb isotopes (upper). Adapted from [36]. Oscilloscope picture of Doppler-broadened absorption spectrum of Rb vapor (lower).

As described before, a double-pass absorption configuration eliminates the Doppler broadening masking, allowing observation of hyperfine transitions as well as crossover resonance effects. The experimental setup for a double-pass setup is shown in Figure 2.7. This setup has thick optics that provides two beams of light, one to provide the saturated absorption signal and one to provide a normalizing beam; the geometry reduces the chances of unwanted reflections; the extra arm has an acousto-optic modulator (AOM) for flexibility of tuning the laser.

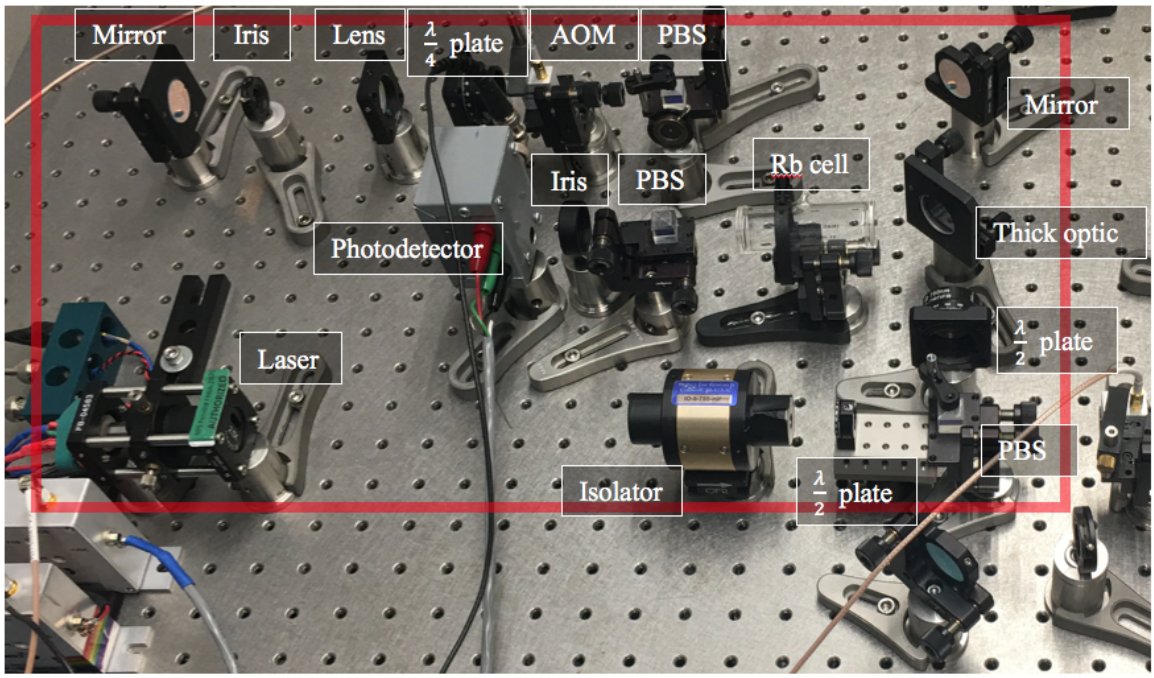

Figure 2.7. Picture of the double-pass saturated absorption setup on optical table.

Performing a frequency scan, over the same cell with ^{85}Rb and ^{87}Rb in their naturally occurring abundance, the absorption spectrum now reflects a saturated absorption spectrum. Figure 2.8 shows the saturated absorption vs frequency for the double-pass configuration. The blue curve shows the absorption spectrum for ^{85}Rb and ^{87}Rb. The excited state transitions are visible as sharp dips, as are the crossover resonances. As expected, comparing with the single-pass configuration in Figure 2.6 (bottom), more transitions are visible, and Doppler broadening is eliminated. The MATLAB code used to generate this figure is in Appendix A.5.

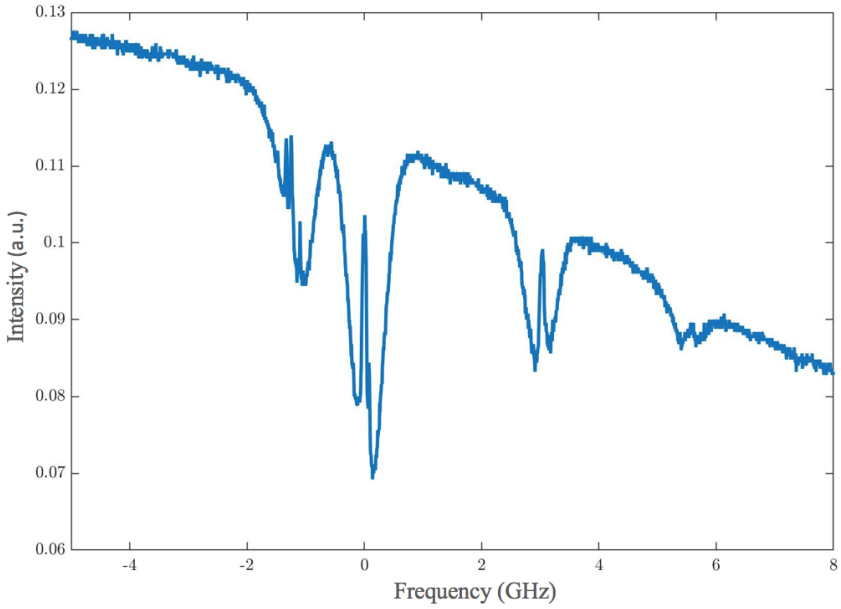

Figure 2.8. Measurement of probe transmission through a cell containing ^{85}Rb and ^{87}Rb isotopes published with MATLAB-R2017a.

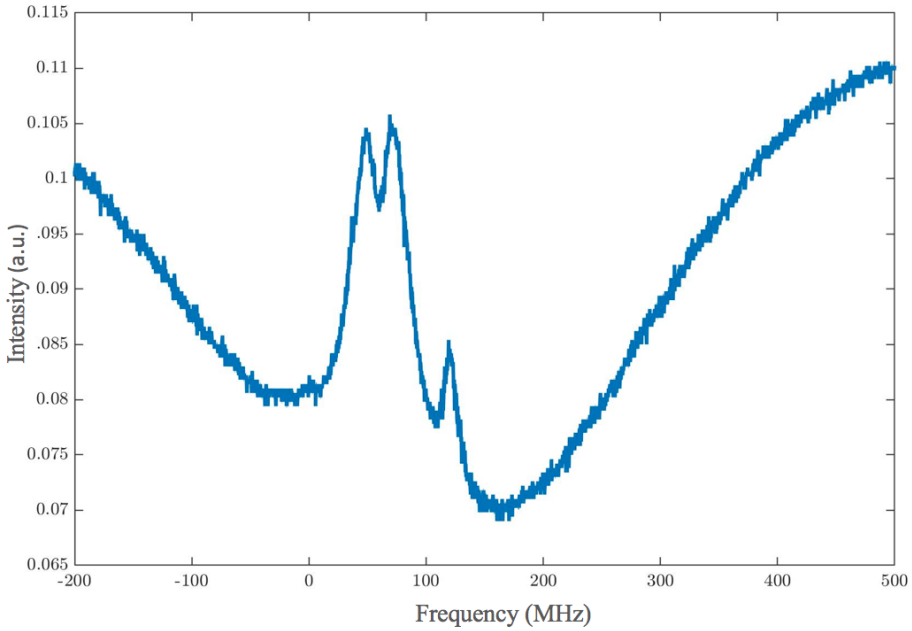

Figure 2.9. Measurement of probe transmission through the red transition of ^{85}Rb.

Since the transitions are visible without Doppler broadening, the laser can be “locked”, i.e. electronically controlled to maintain one single, steady frequency. Depending on which transition is desired, a scan over a smaller frequency range can be conducted in order to determine the exact frequency on which to “lock the laser”. Figure 2.9 shows the red transition of the ^{85}Rb, where the laser will be locked for the squeezing experiment.

CHAPTER 3:
Noise Measurement

Recall that the fundamental noise in an optical beam is called "shot noise" or "quantum noise." Quantum noise in optical beams comes from the quantization of the electromagnetic field, a concept introduced by Paul A. M. Dirac in 1927 [37]. Even in the absence of all other noise sources, a photo-electrically detected coherent light beam still exhibits quantum noise.

According to the laws of quantum mechanics, the total amount of noise in a laser beam cannot be below this shot-noise. However, optical fields have "quadratures" denoted by $\Delta\hat{X}$ and $\Delta\hat{Y}$, which are dimensionless electric field quadratures (analogous to a harmonic oscillator's momentum and position). The quadratures must obey the uncertainty relation $\Delta\hat{X}\Delta\hat{Y} \geqslant 1/4$. While the product of noise quadratures is always greater or equal to 1/4, an individual noise quadrature can be less than 1/4, at the other quadrature's expense being greater than 1/4.

The research objective is to generate squeezed light–the condition in which one property of a laser's noise is below the quantum noise. To verify that the light noise is squeezed, the photodetectors must be capable of detecting signal levels at and below the quantum noise. When a photodetector can measure shot-noise, it is said to be "shot-noise limited."

3.1 Shot-Noise Calculation

For a beam with power P and wavelength λ, the photon rate in photons per seconds is given by

$$n = \frac{P\lambda}{hc}, \tag{3.1}$$

where h is Planck's constant, and c is the speed of light.

The number of photons detected in a given time interval, however, is not constant. For a given time interval t, the average number of photons detected will be nt, where n is the average rate of photons arriving at the detector, and will vary randomly with a standard deviation of $\sqrt{nt}$. As a result, photons collected from a coherent source over a time interval

has a Poissonian statistical distribution [38].

The signal-to-noise ratio (SNR) for a shot-noise limited beam is then defined as

$$SNR = \frac{nt}{\sqrt{nt}} = \sqrt{nt}. \tag{3.2}$$

Since we know our signal power, the shot-noise can be calculated as

$$P_{shot} = \frac{P}{SNR}. \tag{3.3}$$

It is obvious from Equation 3.3 that the shot-noise increases linearly with the laser power. The diode laser used for generating squeezed light has a nominal wavelength of λ = 780 nm. When assuming a laser power of 1 mW, the shot-noise of this laser can be calculated for different time intervals, as shown in Table 3.1.

Table 3.1. P_{shot} with relation of period of time.

Bandwidth detection	Time interval	P_{shot}
1 Hz	1 s	16 pW
1 kHz	1 ms	500 pW
1 MHz	1 μs	16 nW
100 MHz	10 ns	160 nW
150 MHz	6.7 ns	202 nW

The input power of 1 mW can is converted by Equation 3.1 to the number of "noise" photons that a shot-noise limited detection circuit needs to be able to measure. Since the photodetector used in these experiments has a detection bandwidth of 150 MHz, the number of shot-noise photons can be calculated using Equation 3.1. In this case, the number of shot-noise photons is $3.67 * 10^{15}$ corresponding with a shot-noise power of 202 nW.

Since the shot-noise equivalent power is 202 nW at full bandwidth, we must be able to detect less than this amount. The avalanche photodetector (APD) used in this experiment is the Thorlabs model PDA10A, which the manufacturer claims to have a noise-equivalent power (NEP) of $3.5 * 10^{-11}\ W/\sqrt{Hz}$ [39]. NEP is the signal power that gives a signal-to-noise ratio (SNR) of 1 Hz output bandwidth. The photodetector was modified to increase the gain by

ten times, yielding a minimum detectable power is then approximately 42.8 nW. The gain of a photodetector is correlated to its detection bandwidth. By increasing the gain, the full detection bandwidth of the photodetector likely decreased. However, we planned to operate our initial experiments at frequencies well below 15 MHz (the expected bandwidth of the detector with increased gain), so we did not investigate the actual bandwidth further. The result of this preliminary calculation is encouraging since the minimum detectable power is lower than the shot-noise level.

3.2 Shot-Noise Measurement

Theoretically, the APD is shot-noise limited, but it was necessary to verify that the spectrum analyzer could measure power below the shot-noise. Figure 3.1 shows the experimental setup used to detect shot-noise with the spectrum analyzer. A laser beam passes through an optical isolator preventing damage to the laser diode; then, a half-wave plate controls the creation of the superposition of horizontal and vertical polarized light as described in the previous section. The polarized beam splitter then splits the light into vertically and horizontally polarized beams and serves as the intensity regulator. The horizontally polarized beam is then detected by the APD and converted to a voltage. The APD's signal is read on the oscilloscope and a Rohde & Schwarz model FSV7 spectrum analyzer. Detected noise is displayed in dBm as a function of a range of frequencies. A Thorlabs model PM100A power meter was used to measure the laser beam's power, and then the photodetector response was also verified at the oscilloscope.

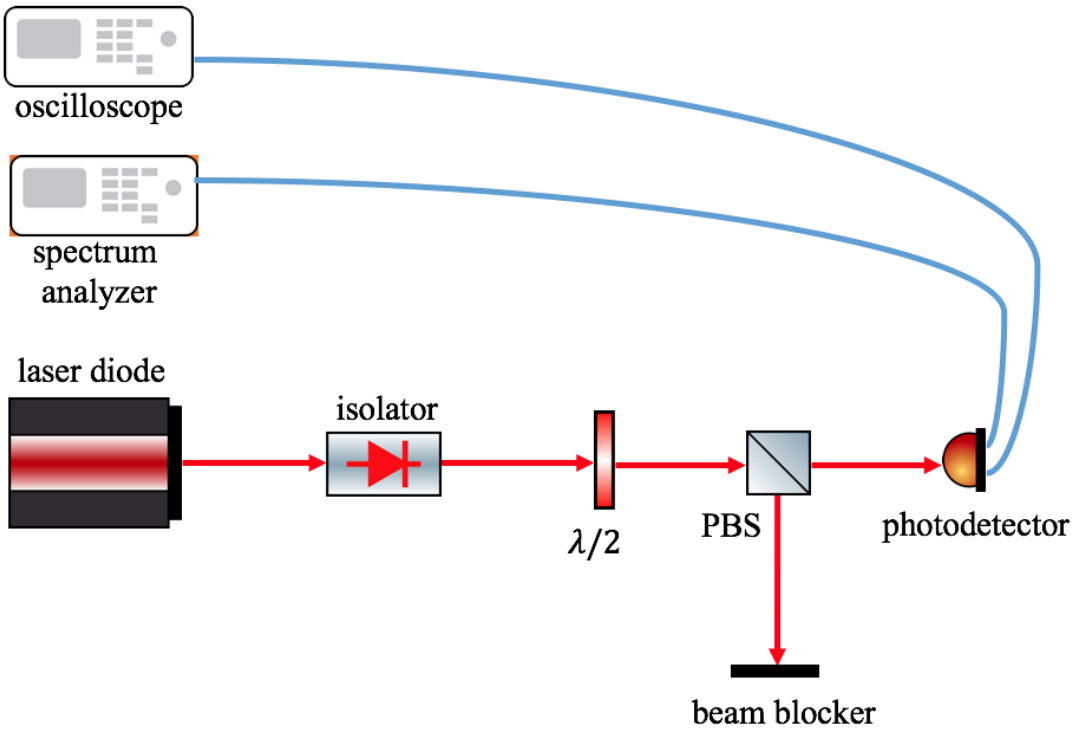

Figure 3.1. Detection setup schematic.

As measured on the oscilloscope, the voltage from the detector corresponds to the optical power of the laser beam. The laser's beam power was arbitrarily set to 24 discreet power levels from 0 mW (no light) to 0.261 mW (a power level below the APD's saturation level) as measured by the PM100A power meter. For each power level, the spectrum analyzer performed a frequency scan from 0 to 2 MHz. These scans at each power level were completed 20 times each and averaged. Plots of each of the average power levels are shown in Figure 3.2. The noise power in dBm on the y-axis shows an anticipated 1/f noise (commonly observed in electronics) [40]. As expected, the noise power increases with optical power.

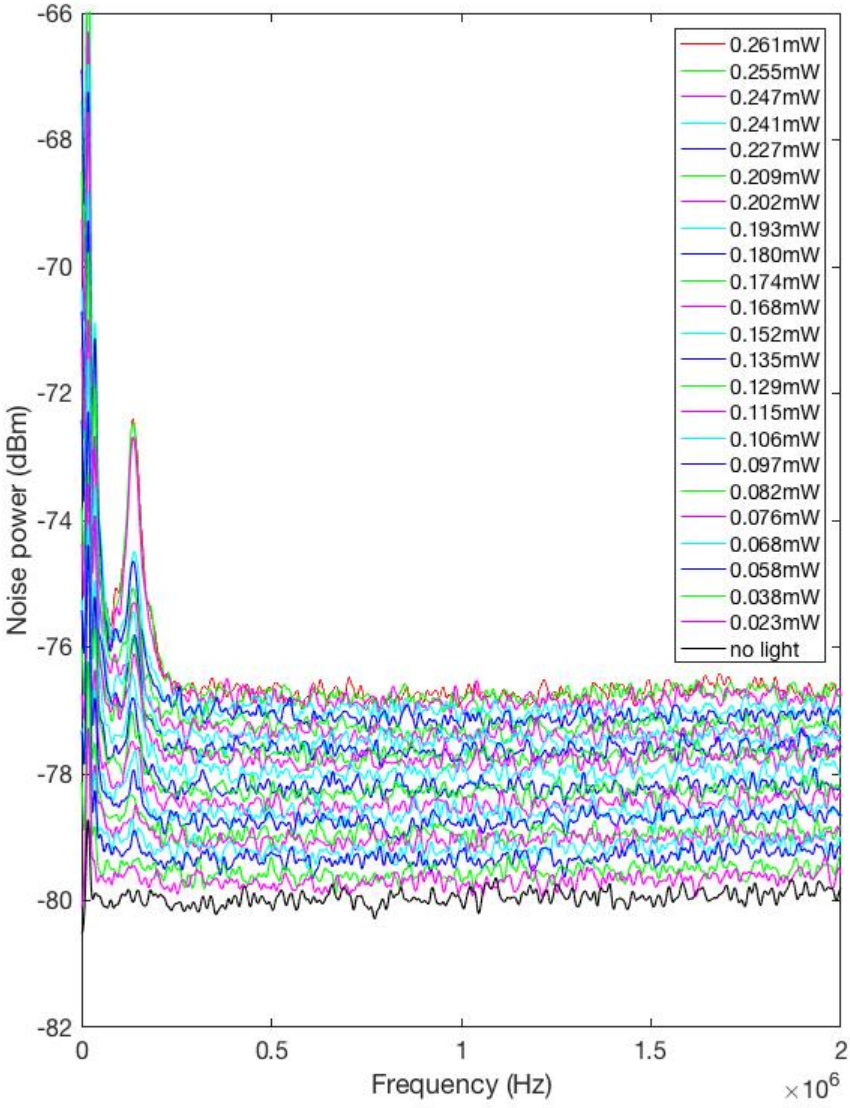

Figure 3.2. Excitation of the detector with gradually increased optical signal.

As shown in Equation 3.3, theoretically, the noise power increases linearly with optical power for a given detection frequency. The spectrum analyzer signal at 1 MHZ (chosen arbitrarily) was extracted for all the selected optical power intensities. Figure 3.3 shows the noise power at 1 MHz vs. the optical noise power. Since the spectrum analyzer collects the

noise power data in decibel-milliwatts, and it was converted to milliwatts by the formula $P(mW) = 1W * 10^{(P_{dBm}/10)}/100000$. It is clear from the best fit line plotted in Figure 3.3 that noise power does indeed increase linearly with optical power, as predicted for a shot-noise limited system. The small deviations from linear behavior result from averaging the noise measurements and not taking the optical power and noise measurement simultaneously.

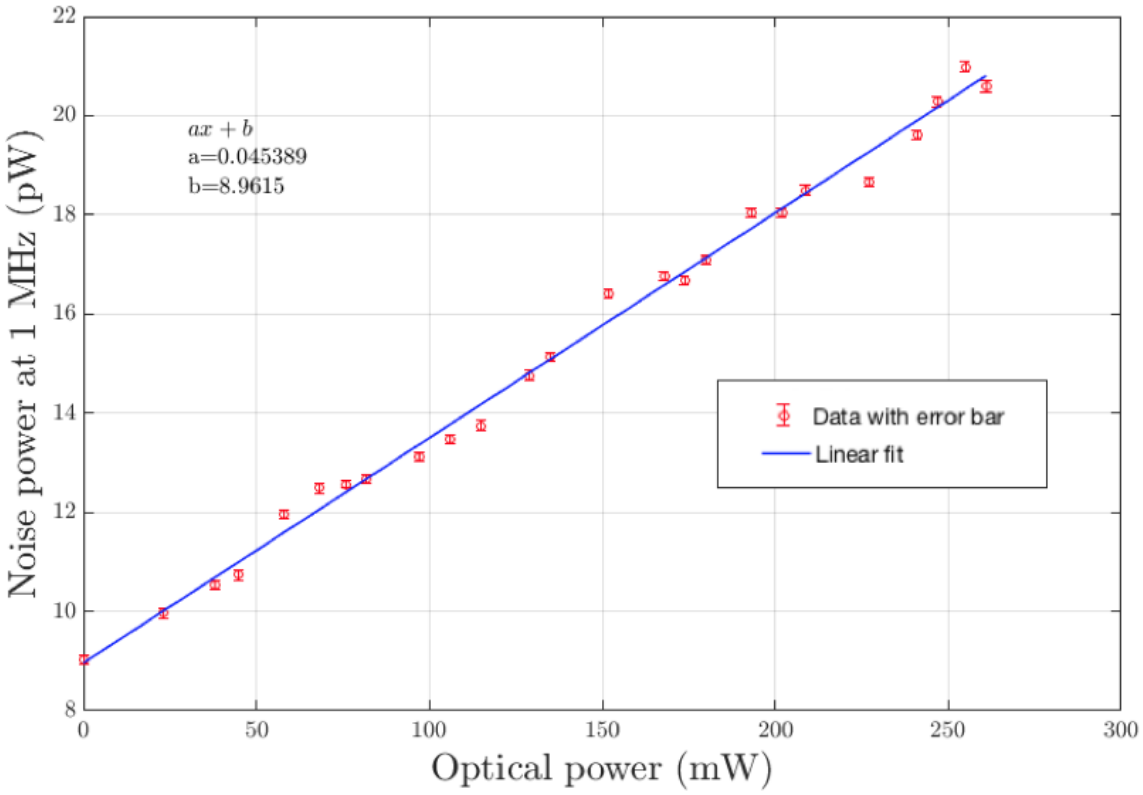

Figure 3.3. Optical power versus noise power at 1 MHz. Error bars represent the standard deviation of the trace from the spectrum analyzer from 15% of the span to 85% of the span (to avoid edge effects like 1/f noise).

We observed that the noise power increases with the optical power, and the best fit for the data is a linear fit, which is characteristic of shot-noise operation. If technical noise were to dominate, then quadratic behavior would be observed. As a stepping stone to a squeezed-light demonstration, excess quantum noise near an atomic resonance was investigated.

3.3 Excess Noise Experiment

Four-wave mixing (FWM), a process that produces the amplitude-squeezed beam, is performed in an atomic Rb vapor containing cell, a nonlinear medium. The Rb vapor is expected to interact non-linearly with the strength of the laser [40]. Due to these non-linearities, correlated beams are generated and therefore squeezing results. However, the noise increase resulting from the added noise from an atomic transition could significantly reduce the squeezing amount achieved by the FWM process. Thus, it is necessary to determine how much noise is added to the laser due to its resonant interaction with Rb vapor.

In the FWM process, the laser beam and unpopulated vacuum side modes enter the cell. The near-resonant laser excites the atom which then spontaneously decays, adding photons into all the side modes within the natural bandwidth [26] of the transition. The amplitude of the beating between the pump and the vacuum side modes increases with an increased number of photons in the vacuum mode. The maximum amplitude of the beating is expected to occurs when the pump laser is not exactly on-resonance but approximately one linewidth detuned either side of the resonance [41]. As depicted in Figure 3.4, the excess noise photons do not populate onto to the pump beam, but instead populate onto vacuum side-modes.

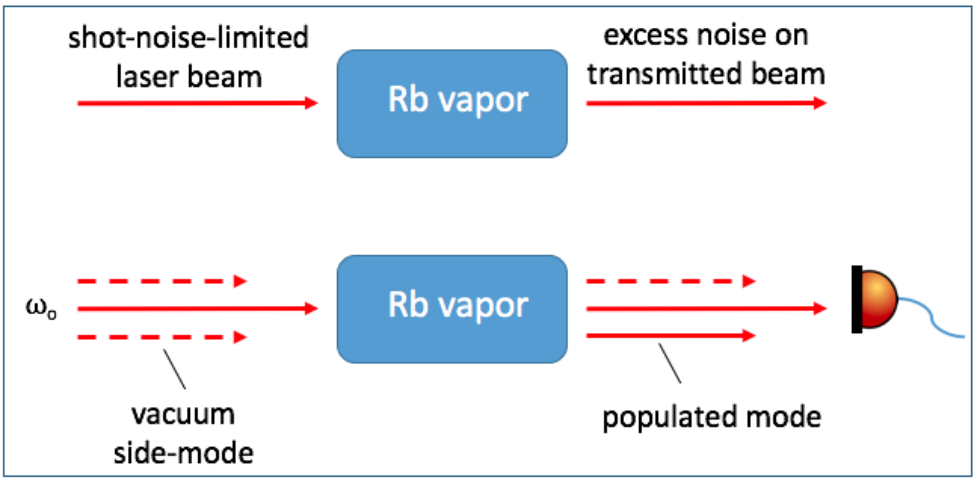

Figure 3.4. Noise characteristics of a laser beam before and after passing through (upper). Laser beam and vacuum side modes at a frequency ω_o passing through Rubidium atoms vapor. Photons populate one or both vacuum sides through FWM, which results in excess noise in the detector photocurrent (lower). Adapted from [42].

The excess noise acquired by a laser beam propagating through atomic vapor can be determined experimentally [42]. An experiment was performed with a Rubidium cell containing ^{85}Rb and ^{87}Rb isotopes. The setup for the excess noise experiment consists of the laser source, the isolator, half-wave plate, beam splitter, Rb cell wrapped with a heating strip, and the photodetector, as shown in Figure 3.5.

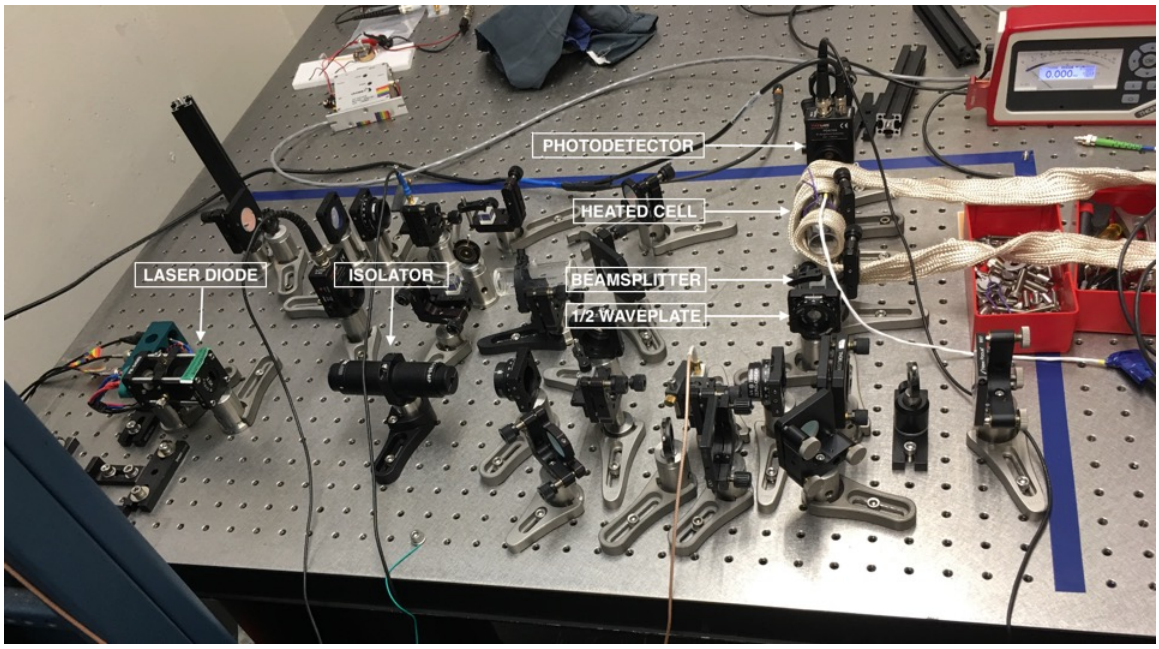

Figure 3.5. Excess noise experiment setup on optical table.

The experiment consists of the transmission of a shot-noise limited laser beam through a cell heated to 41°C (containing ^{85}Rb and ^{87}Rb vapor) and its measurement by a photodetector. An oscilloscope and a spectrum analyzer receive the photodetector output signal. For analysis ease, the spectrum analyzer settings were unchanged during the experiment. Spectrum analyzer settings are shown in Table 3.2.

Table 3.2. Spectrum analyzer settings for data collection

Setting	Value
Sweep time (SWT)	100 ms
Resolution bandwidth (RBW)	10 kHz
Video bandwidth (VBW)	30 Hz
Sweep count	50
Sweep points	2000
Range	log 50 dB

The data was taken on the spectrum analyzer set to zero-span. For zero-span, the frequency is fixed, and the analyzer shows power in dBm as a function of time. Data were collected for four different analyzer frequencies (0.5 MHz, 1 MHz, 5 MHz, and 10 MHz). At each frequency, data was collected for three different shot-noise limited laser powers (0.15 mW, 0.36 mW, and 0.97 mW), as well as without a laser (for baseline measurement). The MATLAB code that plots probe beam transmission (taken by the oscilloscope) and the excess noise power acquired by the laser during its transmission through the hot cell (taken by the spectrum analyzer) is shown in Appendix A.4.

The experiments for 0.5 MHz, 1 MHz, 5 MHz, and 10 MHz are shown in Figures 3.6, 3.7, 3.8, and 3.9, respectively. Each figure shows the curves of the power transmitted for each laser intensity and also its transmission profile (the highest power was chosen to show better definition of the resonance transitions) is plotted. We can observe an increase in the detector's noise at the sides of the resonance, with dips still occurring on resonance. The on-resonance dip is expected because ordinary absorption causes a dip in detected intensity. But we see an increase off to the sides of the resonance, caused by increased quantum noise as discussed.

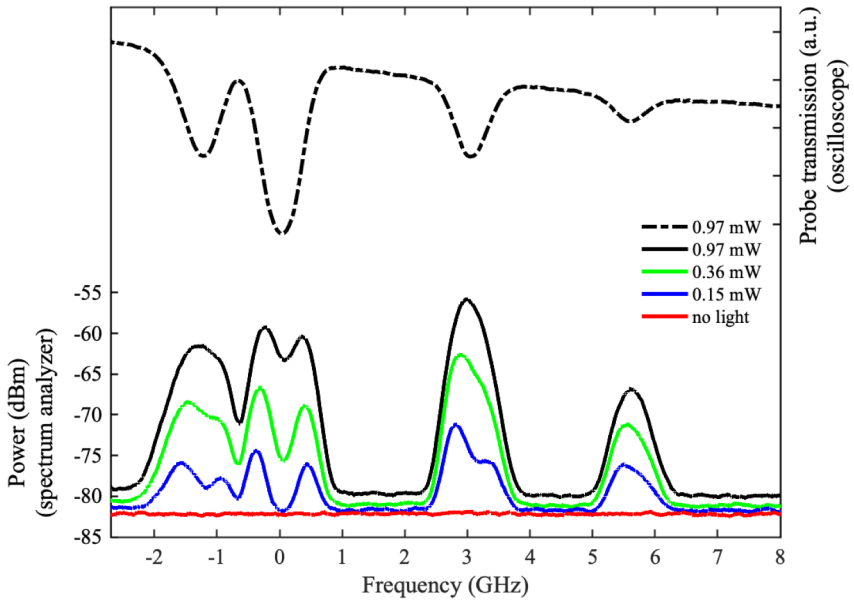

Figure 3.6. Experimental measurements of the transmitted laser beam power through a cell heated at 41°C at three intensity levels at 0.5 MHz.

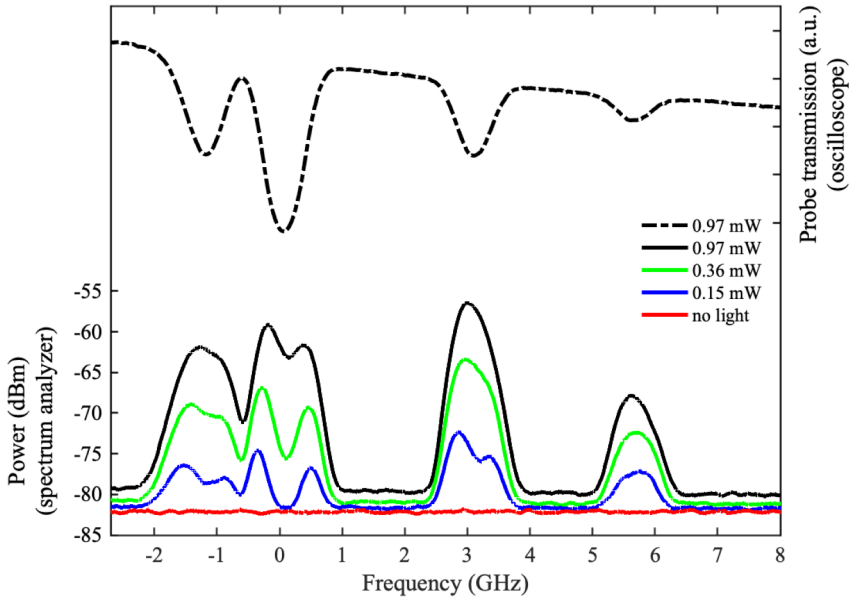

Figure 3.7. Experimental measurements of the transmitted laser beam power through a cell heated at 41°C at three intensity levels at 1 MHz.

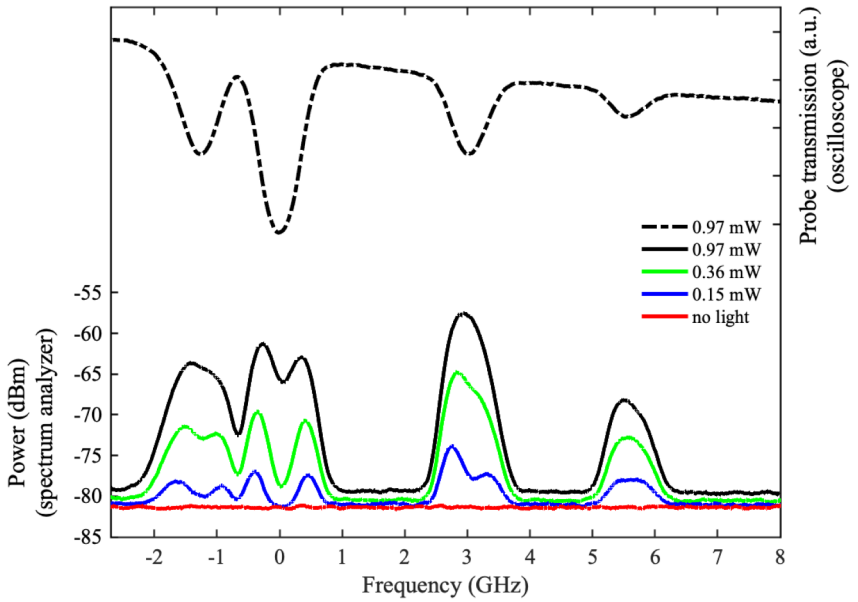

Figure 3.8. Experimental measurements of the transmitted laser beam power through a cell heated at 41°C at three intensity levels at 5 MHz.

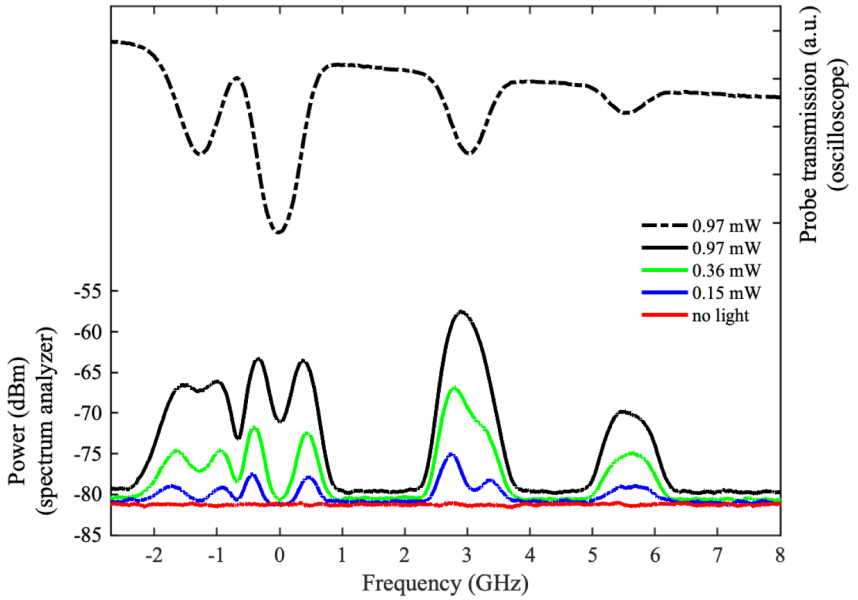

Figure 3.9. Experimental measurements of the transmitted laser beam power through a cell heated at 41°C at three intensity levels at 10 MHz.

The excess noise measurement is relevant because the generated squeezed light in the FWM process could have its noise reduced (squeezed) property attenuated by the noise acquired by the beam during the process. Therefore, before conducting the squeezing experiment in the heat cell containing ^{85}Rb, the excess noise should be measured at the required pump intensity.

3.4 Computational Simulation–Quantum Theory of Excess Noise

Following [42], it is desired to compare the excess noise experimental data to a theoretical simulation. However, the theory predicted in [42] is exceptionally complicated. We desired to develop a simpler model to guide intuition, even if it does not entirely match the experiment. A MATLAB simulation A.3 was created from a theoretical analysis of a system made up of a single-mode laser, two-level atoms, emitted and absorbed photons, and a vacuum mode. Initially, attempts were made to derive excess noise using two vacuum side-modes like [42], but the analytical complexity did not add significant understanding of the physical problem. As a result, the excess noise derivation was based on a single vacuum side-mode.

The basic analysis began with the interaction Hamiltonian, which is the energy operator that accounts for an atom's interaction inside an electric field. The Schrödinger equation in the interaction picture is (see Appendix A.1)

$$\frac{d}{dt}\psi_{int}(t) = \frac{-i}{\hbar}\hat{\mathcal{H}}_{int}\psi_{int}(t),$$

where $\psi_{int}(t)$ is the quantum system state vector, $\hbar$ is Planck's constant, and $\hat{\mathcal{H}}_{int}$ is the interaction Hamiltonian.

This interaction Hamiltonian is part of the system Hamiltonian, which also includes the Hamiltonians for the electric field and atoms. The Schrödinger equation is an ordinary differential equation that can be solved numerically when the Schrödinger equation is written in the form $\frac{d}{dt}\psi = L\psi$ (see Appendix A.2 for whole description).

This solution involves the L matrix, which is a matrix whose size and coefficients vary with the laser intensity (number of photons) (see Appendix A.2.1). We used the MATLAB

code (see Appendix A.3) to simulate the transmission of a probe beam through an atomic medium based on the theoretical calculations presented in Appendix A.2 and A.2. Figure 3.10 shows a pump beam with an initial number of ten photons. As the pump interacts with the atoms on resonance frequency, the pump mode lose photons and they are transferred to the vacuum side-mode near resonance frequency, as seen in our experiment. The MATLAB code only considers one vacuum side-mode; it would be computational onerous to have both side-modes and would not add to our understanding of the phenomenon. However, if we did, our plots would show peaks symmetrically spaced about the resonance.

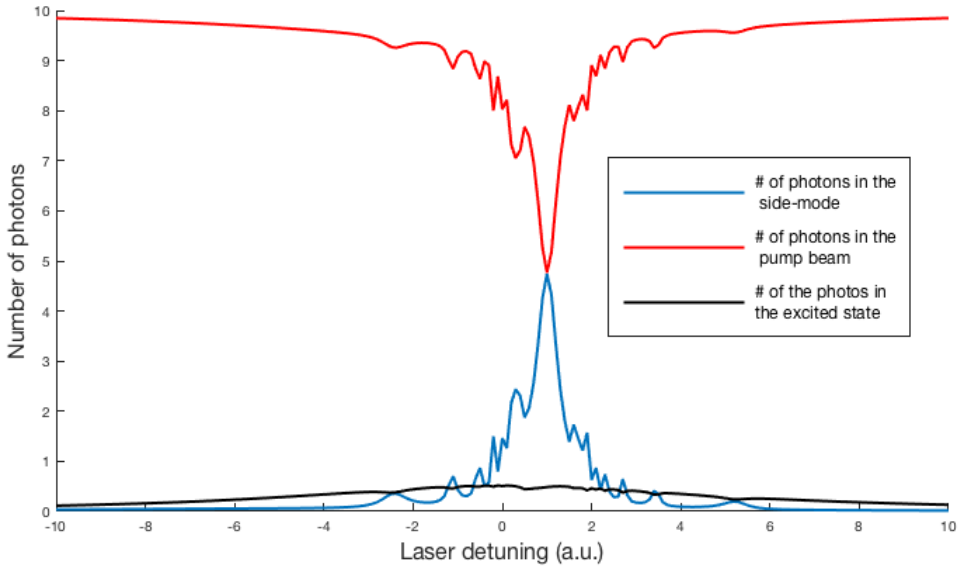

Figure 3.10. Quantum noise observed in a side-mode.

THIS PAGE INTENTIONALLY LEFT BLANK

CHAPTER 4:
Four Wave-Mixing and Squeezing Experiment

4.1 What is Squeezed-Light?

As stated before, quantum noise in light is made up of two quadratures. As a consequence of the Heisenberg uncertainty principle, the total amount of quantum noise remains constant. In 1927, the German physicist Werner Heisenberg introduced the uncertainty principle, which states that there are limits on the precision of simultaneous measurements of a particle's position and velocity in quantum mechanics [25]. Despite the absolute limit on the precision of both simultaneous measurements, improvements in the precision of one of them, to the detriment of the other, is possible without violating the principle.

Light in the mode of on optical field can be imagined as a quantum harmonic oscillator and as such, can be written in terms of momentum and a position. The electric field of coherent light [43] can be described as

$$\hat{E}(\mathbf{r},t) = l(\omega)\boldsymbol{\epsilon}[\hat{a}e^{i(\mathbf{k}\cdot\mathbf{r}-\omega t)} + \hat{a}^{\dagger}e^{-i(\mathbf{k}\cdot\mathbf{r}-\omega t)}], \tag{4.1}$$

where $l(\omega)$ is a real function of frequency, $\boldsymbol{\epsilon}$ is electric field polarization vector, $\hat{a}$ and $\hat{a}^{\dagger}$ are annihilation and creation operators, $\mathbf{k}$ is a wave vector, $\mathbf{r}$ is the position vector, ω is the angular frequency and t is time.

$\hat{X}_1$ and $\hat{X}_2$ are complimentary dimensionless variables called "field quadratures" that obey the uncertainty principle. Those field quadratures are defined as

$$\begin{aligned} \hat{X}_1 &= \hat{a}^{\dagger} + \hat{a} \\ \hat{X}_2 &= i(\hat{a}^{\dagger} - \hat{a}). \end{aligned} \tag{4.2}$$

For coherent states, $\Delta X_1 \cdot \Delta X_2 = \frac{1}{4}$

Substituting $\hat{X}_1$ and $\hat{X}_2$ back in the Equation 4.1, the oscillating field can be decomposed as

$$\hat{E}(\mathbf{r},t) = l(\omega)\epsilon[\hat{X}_1 cos(\mathbf{k}\cdot\mathbf{r}-\omega t) - \hat{X}_2 sin(\mathbf{k}\cdot\mathbf{r}-\omega t)]. \tag{4.3}$$

For squeezed states, the product of the quadrature variances is still the Heisenberg minimum uncertainty, but the variances are not equal. One variance will be smaller (or squeezed), and the other will increase. A visualization of the electric field in coherent and squeezed states is shown in Figure 4.1. In (a), the electric field is in a coherent state in which the product of the noise exhibits minimum uncertainty because the amplitude and phase quadratures, X_1 and X_2 respectively, are equal. In (b), the electric field is shown in a quadrature-squeezed state. In this state, the uncertainty, or variance, in X_1 is reduced, as shown by an ellipse. A quadrature-squeezed state shown in (c), as demonstrated by the reduction in uncertainty in X_2 [20].

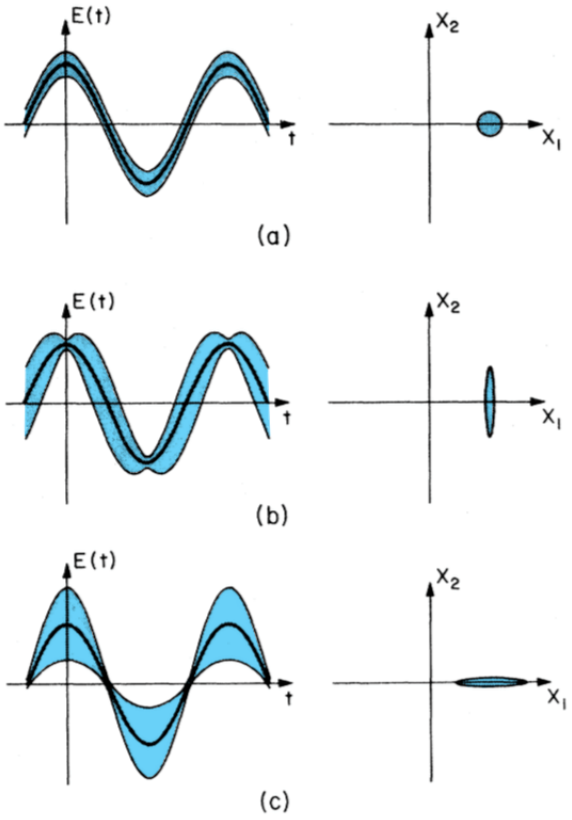

Figure 4.1. Sketches of the electric field versus time are shown in a dark line in three graphs (left side). The blue-shaded bands around the curves indicate the uncertainty for the coherent state. The graph to the right shows the error area in the complex-amplitude plane. Uncertainty for a coherent state (a). States with reduced amplitude uncertainty (b). States with reduced phase fluctuations (c). Adapted from [20].

4.2 Four-Wave Mixing

4.2.1 Non-Linear Media

In the saturation absorption section, we observed the effect of the light on the atoms (pump beam exciting the atoms) and vice-versa (probe beam monitoring the optical properties of the atomic vapor medium). The medium's response to the probe beam is linear when the effect of probe on the atoms' state is negligible. The same can be said when the probe beam drives atoms' transitions without significantly altering its properties such as polarization or intensity. The linearity of the above scenarios is only an approximation since all mutual interactions must respect the conservation of energy and angular momentum [44]. The influence of atoms on the laser and vice-versa depends on the atom density and the laser intensity, as shown in Figure 4.2. Figure 4.2 describes four different laser intensity and particle density scenarios and portrays the influence between the atoms and the lasers.

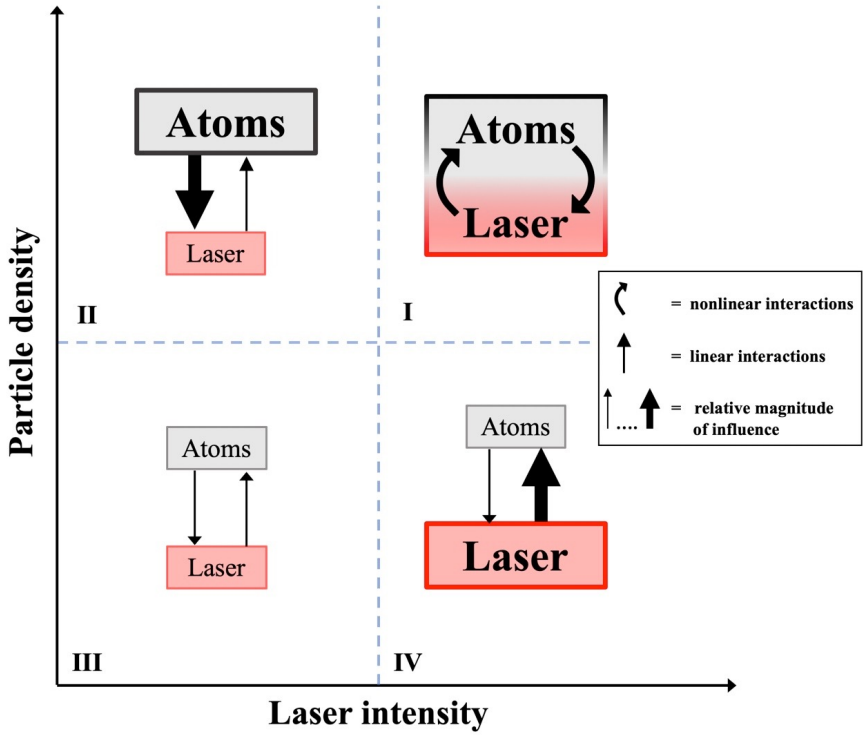

Figure 4.2. Interactions between laser beam and resonant atom media. Adapted from [44].

When the laser intensity and atomic density are low, the influence of one on the other is weak (as shown in quadrant III). Quadrant IV offers the ideal pump laser operation, where its influence in the atomic medium is strong, but the medium effect in the laser is weak. The ideal probe operation is shown in quadrant II, where the laser has a weak influence in the medium, but such as the excess noise measurements, the medium has a strong effect on the laser. Quadrant I shows strong non-linear mutual interactions between the laser and the resonant atom medium, as a result of nonlinear susceptibility [45], where susceptibility, χ, is the dimensionless constant of proportionality that describes the how polarized a medium becomes when an electric field is applied [46].

In a linear medium, the interaction between the medium and the different waves are independent of each other. If a system of multiple lasers and a resonant atomic medium is operating in the non-linear region, the atoms cause interactions between each of the waves. This interaction is called wave mixing [44].

4.2.2 Four-wave mixing

When a probe and pump cross each other at a small angle within a non-linear atomic medium, a third, new wave, called the conjugate beam, can be produced. The conjugate beam quantum related with the probe. The four-wave mixing technique produces this phenomenon by generating the desired quadrature squeezed beam [47]. This squeezed beam can then be used as the detection beam in an atomic interferometer.

Multiple experimental setups can employ the four-wave mixing technique. Among the different designs is the double-Λ configuration using ^{85}Rb as the non-linear medium. A simplified representation of the double-Λ structure is shown in Figure 4.3. The red ν_1 represents a linearly polarized probe beam, while the orange ν_p represents a much stronger, horizontally polarized pump beam. The conjugate, or the generated wave, is shown in blue as ν_2.

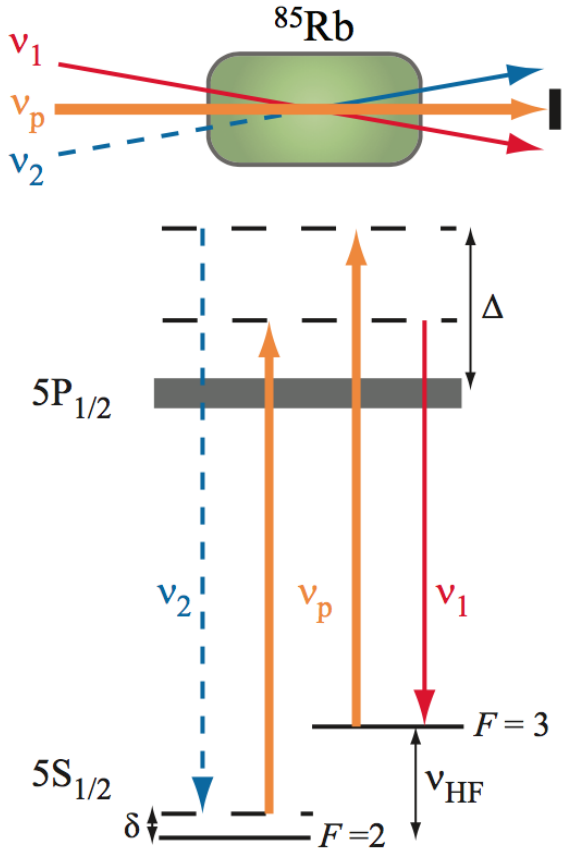

Figure 4.3. FWM double-Λ configuration. Source: [48].

Notice that the top image shows a small angle between ν_p and ν_1, which allows necessary phase-matching condition in wave mixing to occur. During this process, the probe beam (ν_1) is amplified, and the generated conjugate beam (ν_2) is quantum-correlated to the probe beam. "Quantum-correlated" in this case refers to the fact that the photons in the squeezed beam (ν_2) come from the probe beam (ν_1), even though they are spatially separated, and the measurements of photons in each beam are correlated [49]. This phenomenon is only observed in quantum physics.

The bottom image shows the atomic transitions for ^{85}Rb from energy levels F to virtual excited states represented by the dashed lines. Δ is the difference between the highest virtual state and the excited state $5P_{1/2}$. Two photons are absorbed from the pump beam v_p, where one photon amplifies the probe beam, and the other creates the quantum-correlated

conjugate beam [48].

This FWM technique will be used in an experiment to generate quadrature squeezed that will be used in the AIL interferometer. The experimental setup utilizing the FWM process is shown in Figure 4.4.

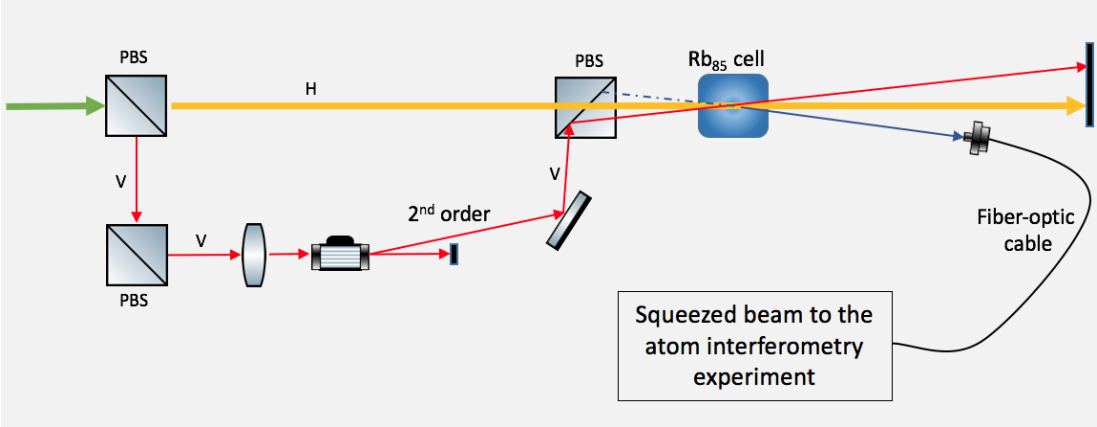

Figure 4.4. Schematic of a experiment setup for a FWM with a double-Λ configuration.

Imagine a laser beam whose frequency is "locked" with the reference saturated absorption setup. This laser travels through a fiber optic and enters as the green arrow shown on the left side of Figure 4.4. The laser enters free space before getting split by a polarizing beam splitter (PBS). The PBS separates the beam in two beams: a vertically polarized and a horizontally polarized beam. The horizontally polarized beam will be the stronger beam, or "pump" beam (ν_p). The pump beam goes to the hot vapor ^{85}Rb cell, which will behave as a non-linear media as discussed in Subsection 4.2.1.

The weak, vertically-polarized probe beam is directed via a PBS and mirror to a plano-convex lens that will focus the laser at the lens's focal point. A free-space, acousto-optic frequency shifter (AOFS) is placed at the focus point of the lens. The AOFS needs to be angled at the exact Bragg angle relative to the laser to create a diffracted light. The diffracted light will have its frequency either increased or decreased by an amount equal to the RF carrier frequency depending on the angle of the modulator [40]. The non-refracted beam is called the zeroth-order beam. The diffracted beam is called the first-order beam, and it has a lower intensity than the zeroth-order beam, as shown in Figure 4.5. When the AOFS is

angled to 2 times the Bragg angle, a second-order beam (with double the frequency shift and lower intensity than the first order) appears. The intent is to generate a second-order beam because it would have a 3 GHz (two times 1.5 GHz, which is the frequency that the AO modulator is driven) frequency shift. The 3 GHz frequency shift is the (ν_{HF}) shown in 4.4, which represents the frequency difference between $5S_{1/2}$ levels F=2 and F=3. The zeroth-order beam is blocked, and the frequency-shifted beam is now the probe beam (ν_1). The probe (ν_1) is then directed via a mirror and PBS to the cell.

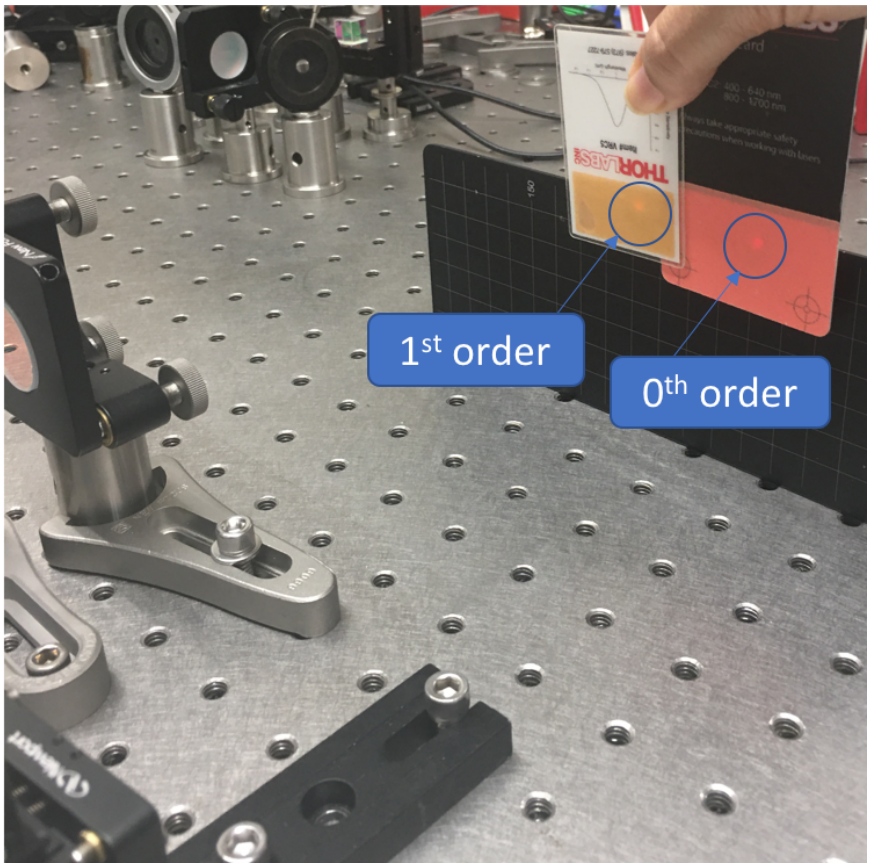

Figure 4.5. Picture of the 0^{th} order beam and the 1^{st} order diffracted beam from the AOFS.

The probe beam and the pump beam then go through the cell and intersect at a small angle. At this intersection, both beams will interact with the same group of atoms. This interaction generates the quadrature-squeezed beam that is sent to another fiber optic that directs the beam to the AIL interferometer, where it will be used as a detection laser. Implementation

of this design is in progress as shown in Figure 4.6.

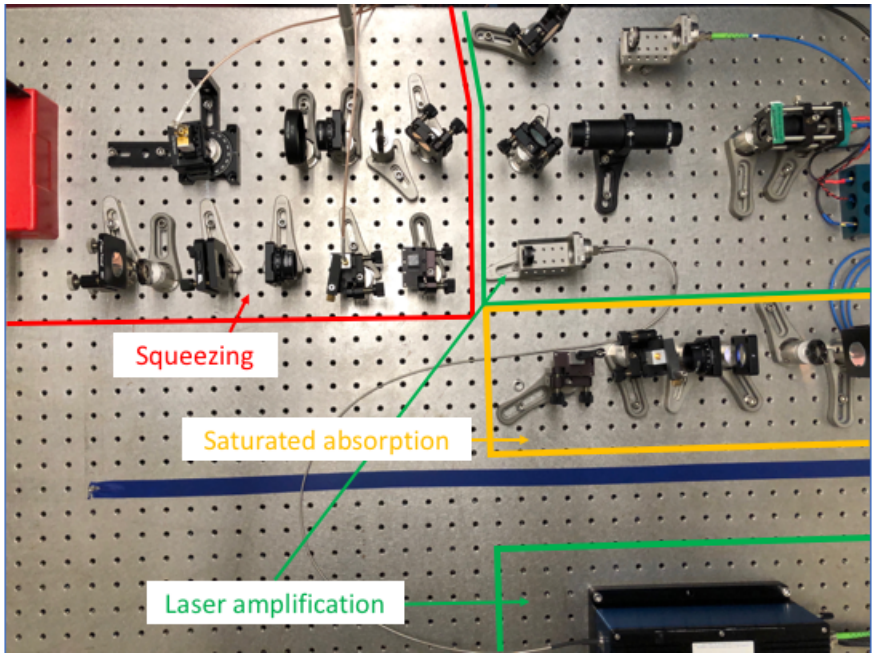

Figure 4.6. Picture of current setup at the lab.

The optical table is divided into three parts: the laser amplification section (in green), the saturated absorption section (in yellow), and the squeezing section. The saturated absorption is not complete. It had to be moved to provide space for the amplification area and is now under construction once more. The laser power is amplified by a tapered amplifier (Newport - model TA-7600). A PBS splits the beam to provide a beam to the saturated absorption experiment and another (with higher power) to the squeezing (FWM) experiment. The squeezing section splits the laser once more. One beam will be the pump, and the other beam undergoes a double frequency shifting to became the probe laser. Both beams will intercept inside the ^{85}Rb cell giving origin to the squeezed-beam.

The future steps to the experiment will be to finish the saturated absorption part and lock the laser. Then in the squeezing section, produce the second-order beam for the FWM process.

CHAPTER 5:
Conclusion

In the event of a long-lasting disruption of the heavily relied upon, satellite-driven GPS, there is a need for inertial navigation sensors that guarantee secure and precise navigation. Of all INS sensors, atom interferometers show great promise to deliver precise positioning measurements.

The experimental NPS atom interferometer can be improved by using a detection laser with unique characteristics, like quadrature-squeezed noise. This thesis laid the groundwork for developing this quadrature-squeezed beam through the FWM process by presenting a conceptual understanding of the physics and by performing preliminary experiments.

First, a single-pass absorption experiment was built. The laser and the isolator were aligned, and the Doppler broadening effect was demonstrated. Single absorption spectroscopy identified two Doppler broadened transitions in each of ^{85}Rb and ^{87}Rb isotopes. Later, a Doppler-free double-pass saturated absorption experiment was set up to observe hyperfine transitions. Identification of these transitions is necessary in order to "lock the laser," which is the process that fixes the laser to a chosen frequency that will "drive" an atomic transition. Locking the laser is recommended as a future experiment in order to measure the atom populations.

Second, experiments measuring quantum noise were performed. It was discussed that the quadrature-squeezed light is a light that exhibits a noise level below the quantum noise, also called "shot-noise." By ensuring that the photodetector detects the shot noise and the spectrum analyzer measures it, the squeezed noise's amplitude could be measured. The theoretical linear relationship between optical power and noise power was demonstrated. Generation of a squeezed light through the FWM process has a drawback in that the non-linear medium utilized in the process generates noise. This excess noise could negate any squeezed-noise advantages. This non-linear medium generated excess noise was observed through experimentation by transmitting the laser through a hot atomic vapor cell. The results agreed with previous research [41]. A theoretical treatment and simulation of the excess noise phenomenon was presented.

Finally, an experimental setup for generation of amplitude-squeezed light using the FWM process was designed. The intent of this design is to drive the F = 3 $\rightarrow$ F'= 4 of the D2 transition of ^{85}Rb in order to meet the specifications of the NPS atom interferometer. Follow on research should utilize this design to complete the FWM experiments.

When the experiment is complete, we expect the generated quadrature-squeezed light will improve the AIL atom interferometer's sensitivity for detecting path length differences in atomic waves. Such an improvement will result in more precise inertial sensing compared to current systems in use today, like ring-laser gyros. Any INS will inherently accumulate errors in measurement throughout its operation; therefore, a system with higher precision will result in smaller errors. Thus, the atom interferometer has the potential to offer a reliable and accurate alternative to other INS and to GPS, which is susceptible to environmental and man-made disruptions.

APPENDIX: Theoretical Derivations and MATLAB Codes

A.1 Interaction Hamiltonian

We are interested in investigating the interaction between the single-mode laser beam (electric field), two-level atoms, emitted and absorbed photons, and the vacuum mode. Therefore, the interaction of light and matter should be described as an entire system. Let's start defining a Hamiltonian, the energy operator, for this system,

$$\mathcal{H} = \mathcal{H}_{field} + \mathcal{H}_{atom} + \mathcal{H}_{int} = \mathcal{H}_0 + \mathcal{H}_{int}, \tag{A.1}$$

where $\mathcal{H}_{field}$ is the light field Hamiltonian, $\mathcal{H}_{atom}$ is the atom Hamiltonian and $\mathcal{H}_{int}$ is the light-matter interaction Hamiltonian. Also, the sum of $\mathcal{H}_{field}$ and $\mathcal{H}_{atom}$ is called the bare Hamiltonian $\mathcal{H}_o$.

The interaction Hamiltonian is the energy operator that describes the interaction of an atom placed inside an electric field $\hat{E}$. The atom, electrically neutral as a whole, has it charged regions: nucleus and electron cloud influenced by the electric field. The charged regions are pushed apart by the electric field and act as a dipole [46]. In the Schrödinger picture, operators correspondent to observables is time-independent, while the state vectors evolve in time. [50]. The interaction Hamiltonian in the Schrödinger picture can be described as

$$\mathcal{H}_I = -\hat{\mu} \cdot \hat{E}(\mathbf{r}, t), \tag{A.2}$$

where $\hat{\mu}$ is the electric dipole moment vector operator and the $\hat{E}(0, \mathbf{r})$ is electric field.

The quantization of the electric field is expressed as [51] as,

$$\hat{E}(\mathbf{r}, t) = \frac{i}{2\sqrt{\epsilon_o} L^{3/2}} \sum_{ks} \{[\omega \hat{q}_{qs}(t) + \hat{p}_{qs}(t)] \hat{\epsilon}_{ks} e^{i\mathbf{k}\cdot\mathbf{r}} - c.c., \tag{A.3}$$

where L is the side of a large cube that contains the electromagnetic field (which eventually

will be taken to be infinite), ϵ_o is the vacuum dielectric constant, $\mathbf{k}$ is a wave vector, s is a polarization index and $\mathbf{r}$ is the position vector. $q_{qs}(t)$ and $p_{qs}(t)$ are momentum and position variables that oscillate sinusoidally in time at frequency ω.

Furthermore, the book also defines the non-Hermitian creation and annihilation operators as

$$\hat{a}^{\dagger}_{ks}(t) = \frac{1}{(2\hbar\omega)^{1/2}}[\omega\hat{q}_{qs}(t) + \hat{p}_{qs}(t)]$$
$$\textit{and} \tag{A.4}$$
$$\hat{a}_{ks}(t) = \frac{1}{(2\hbar\omega)^{1/2}}[\omega\hat{q}_{qs}(t) - \hat{p}_{qs}(t)].$$

Substituting equations A.4 into the quantized electrical field equation A.3 we obtain

$$\hat{E}(\mathbf{r},t) = \frac{i}{2\sqrt{\epsilon_o}L^{3/2}}\sum_{ks}\{(2\hbar\omega)^{1/2}\hat{a}_{ks}\hat{\epsilon}_{ks}e^{i\mathbf{k}\cdot\mathbf{r}} - (2\hbar\omega)^{1/2}\hat{a}^{\dagger}_{ks}\hat{\epsilon}_{ks}e^{-i\mathbf{k}\cdot\mathbf{r}}\}. \tag{A.5}$$

Defining

$$l(\omega_{ks}) = i\sqrt{\frac{\hbar\omega_{ks}}{2\epsilon_0}}$$

and considering that in the problem of excess noise we are dealing with two modes: the pump laser beam and the initially vacuum mode; observing at the origin (r = 0); the equation A.5 becomes

$$\hat{E}(0,t) = \frac{1}{L^{3/2}}(l(\omega_1)\hat{a}_1\epsilon_1 + l^{\dagger}(\omega_1)\hat{a}^{\dagger}_1\epsilon^{\dagger}_1 + (l(\omega_2)\hat{a}_2\epsilon_2 + l^{\dagger}(\omega_2)\hat{a}^{\dagger}_2\epsilon^{\dagger}_2). \tag{A.6}$$

Now that we have the quantized electric field, let us return to the interaction Hamiltonian $\mathcal{H}_{int}$ (A.2) and substitute the electric field (A.6) into it

$$\mathcal{H}_{int} = -\frac{(\mu_{12}\cdot b + \mu^{\dagger}_{12}\cdot b^{\dagger})}{L^{3/2}}\cdot(l(\omega_1)\hat{a}_1\epsilon_1 + l^{\dagger}(\omega_1)\hat{a}^{\dagger}_1\epsilon^{\dagger}_1 + (l(\omega_2)\hat{a}_2\epsilon_2 + l^{\dagger}(\omega_2)\hat{a}^{\dagger}_2\epsilon^{\dagger}_2) \tag{A.7}$$

$$\begin{aligned}\mathcal{H}_{int} = -\frac{1}{L^{3/2}}[&l(\omega_1)(\mu_{12}\cdot\epsilon_1)ba_1 + l^\dagger(\omega_1)(\mu_{12}\cdot\epsilon_1^\dagger)a_1^\dagger b + l(\omega_2)(\mu_{12}\cdot\epsilon_2)ba_2 + \\ &l^\dagger(\omega_2)(\mu_{12}\cdot\epsilon_2^\dagger)a_2^\dagger b + l(\omega_1)(\mu_{12}^\dagger\cdot\epsilon_1)b^\dagger a_1 + l^\dagger(\omega_1)(\mu_{12}^\dagger\cdot\epsilon_1^\dagger)b_1^\dagger a_1^\dagger + \\ &l(\omega_2)(\mu_{12}\cdot\epsilon_2^\dagger)b^\dagger a_2 + l^\dagger(\omega_1)(\mu_{12}^\dagger\cdot\epsilon_2^\dagger)b^\dagger a_2^\dagger].\end{aligned} \tag{A.8}$$

Using the Rotating Wave Approximation (RWA), the terms depending on $\mu^\dagger\cdot\epsilon^\dagger$ or $\mu\cdot\epsilon$, will average to zero for equation (A.8) time state relevant to experiments. Therefore, those terms were discarded, and only terms slowly varying in time are kept. Therefore, the equation is simplified to

$$\begin{aligned}\mathcal{H}_{int} = -\frac{1}{L^{3/2}}[&l^\dagger(\omega_1)(\mu_{12}\cdot\epsilon_1^\dagger)a_1^\dagger b + l^\dagger(\omega_2)(\mu_{12}\cdot\epsilon_2^\dagger)a_2^\dagger b + l(\omega_2)(\mu_{12}\cdot\epsilon_2)ba_2 + \\ &l(\omega_1)(\mu_{12}^\dagger\cdot\epsilon_1)b^\dagger a_1 + l(\omega_2)(\mu_{12}\cdot\epsilon_2^\dagger)b^\dagger a_2].\end{aligned} \tag{A.9}$$

For simplification, let's call

$$g_i(\omega_l) = -\frac{1}{L^{3/2}\hbar}l(\omega_l)(\boldsymbol{\mu})_{12}^\dagger\cdot\boldsymbol{\epsilon}_i, \tag{A.10}$$

for i=1 (ground level) and 2 (excited level). Then we can rewrite the equation A.9 as

$$\mathcal{H}_{int} = \hbar(g_1 b^\dagger a_1 + g_2 b^\dagger a_2 + g_1^\dagger a_1^\dagger b + g_2^\dagger a_2^\dagger b), \tag{A.11}$$

where $\hat{a}$ is the photon annihilation operator, $\hat{a}^\dagger$ is the photon creation operator, $\hat{b}$ is the atom ladder (lowering) operator, and $\hat{b}^\dagger$ atom raising operator.

A.2 Development of the Schrödinger Equation in the Interaction Picture

Now that we have an equation to the interaction Hamiltonian, we can consider the time evolution of the total Hamiltonian

$$\mathcal{H} = \mathcal{H}_{field} + \mathcal{H}_{atom} + \mathcal{H}_{int} = \mathcal{H}_0 + \mathcal{H}_{int},$$

where

$$\mathcal{H}_{atom} = \hbar\omega_o b^\dagger b$$
$$\mathcal{H}_{field} = \hbar\omega_1 \hat{n}_1 + \hbar\omega_1 \hat{n}_2$$

and $\hat{n}_1$ and $\hat{n}_2$ are the photon number operators for mode 1 (laser), and mode 2 (vacuum).

Using the Unitary Transformation we can write the wavefunction ψ_{int}, which is the wavefunction in the interaction picture as

$$\psi_{int}(t) = e^{\frac{i}{\hbar}\mathcal{H}_o t}\psi_s(t). \tag{A.12}$$

Then,

$$\frac{d}{dt}\psi_{int}(t) = \left(e^{\frac{i}{\hbar}\mathcal{H}_o t}\right)\frac{d}{dt}\psi_s(t) + \frac{i}{\hbar}\mathcal{H}_o\left(e^{\frac{i}{\hbar}\mathcal{H}_o t}\right)\psi_s(t). \tag{A.13}$$

But the Schrödinger's equation in the Schrödinger's picture is

$$\frac{d}{dt}\psi_s(t) = -\frac{i}{\hbar}(\mathcal{H}_0 + \mathcal{H}_{int})\psi_s(t). \tag{A.14}$$

Substituting equation A.14 into A.13 we obtain

$$\frac{d}{dt}\psi_{s(t)} = e^{\frac{i}{\hbar}\mathcal{H}_o(t)}\left(-\frac{i}{\hbar}\right)(\mathcal{H}_0 + \mathcal{H}_{int})\psi_s(t) + \frac{i}{\hbar}\mathcal{H}_o t\psi_s(t) + \frac{i}{\hbar}\mathcal{H}_o\left(e^{\frac{i}{\hbar}\mathcal{H}_o t}\right)\psi_s(t), \tag{A.15}$$

$$\frac{d}{dt}\psi_s(t) = -\frac{i}{\hbar}\left(e^{\frac{i}{\hbar}\mathcal{H}_o t}\right)\mathcal{H}_{int}\psi_s(t). \tag{A.16}$$

Substituting equation A.12 into equation A.14

$$\frac{d}{dt}\psi_{int}(t) = -\frac{i}{\hbar}\left(e^{\frac{i}{\hbar}\mathcal{H}_o t}\right)\mathcal{H}_{int}\left(e^{\frac{-i}{\hbar}\mathcal{H}_o t}\right)\psi_{int}(t). \tag{A.17}$$

Rewriting equation A.12 as an unitary vector and ket form substituting equation A.12 into

equation A.14 we have

$$|\psi_{int}(t)\rangle = U\,|\psi_s(t)\rangle\,. \tag{A.18}$$

Then applying the operator and keeping in mind that $U^\dagger U = 1$

$$\langle\psi_s|\,\hat{A}\,|\psi_s\rangle = \langle\psi_s|\,U^\dagger U\hat{A}U^\dagger U\,|\psi_s\rangle\,. \tag{A.19}$$

For the transformation

$$|\psi_{int}\rangle = U\,|\psi_s\rangle \tag{A.20}$$

we then have

$$\hat{A}_{int} = U\hat{A}_s^\dagger U^\dagger. \tag{A.21}$$

This means that in equation

$$\left(e^{\frac{i}{\hbar}\mathcal{H}_o t}\right)\mathcal{H}_{int}\left(e^{\frac{i}{\hbar}\mathcal{H}_o t}\right) = \mathcal{H}_{ii}. \tag{A.22}$$

So the Schrödinger equation in the interaction picture is

$$\frac{d}{dt}\psi_{int}(t) = \frac{-i}{\hbar}\mathcal{H}_{ii}\psi_{int}(t). \tag{A.23}$$

Give an operator A_s, how does it evolve in the interaction picture? Start with equation

$$A_I = \left(e^{\frac{i}{\hbar}\mathcal{H}_o t}\right)A_s\left(e^{-\frac{i}{\hbar}\mathcal{H}_o t}\right) \tag{A.24}$$

$$\begin{aligned}
\frac{d}{dt}A_I &= \left(e^{\frac{i}{\hbar}\mathcal{H}_o t}\right)\left[-\frac{i}{\hbar}A_s\mathcal{H}_o e^{\frac{i}{\hbar}\mathcal{H}_o t} + \left(\frac{d}{dt}A_s\right)e^{-\frac{i}{\hbar}\mathcal{H}_o t}\right] + \frac{i}{\hbar}\mathcal{H}_o e^{\frac{i}{\hbar}\mathcal{H}_o t}A_s e^{\frac{i}{\hbar}\mathcal{H}_o t} \\
&= -\frac{i}{\hbar}e^{\frac{i}{\hbar}\mathcal{H}_o}A_s\mathcal{H}_o e^{-\frac{i}{\hbar}\mathcal{H}_o t} + e^{\frac{i}{\hbar}\mathcal{H}_o t}\left(\frac{d}{dt}A_s\right)e^{-\frac{i}{\hbar}\mathcal{H}_o t} + \frac{i}{\hbar}(e^{\frac{i}{\hbar}\mathcal{H}_o t})\mathcal{H}_o A_s e^{-\frac{i}{\hbar}\mathcal{H}_o t} \\
&= -\frac{i}{\hbar}e^{\frac{i}{\hbar}\mathcal{H}_o}[A_s,\mathcal{H}_o] + e^{-\frac{i}{\hbar}\mathcal{H}_o t} + e^{\frac{i}{\hbar}\mathcal{H}_o t}\left(\frac{d}{dt}A_s\right)e^{-\frac{i}{\hbar}\mathcal{H}_o t}.
\end{aligned} \tag{A.25}$$

Since A_s is not explicit time dependent, $\frac{d}{dt}A_s = 0$,

$$\begin{aligned}\frac{d}{dt}A_I &= -\frac{i}{\hbar}e^{-\frac{i}{\hbar}\mathcal{H}_o t}A_s\mathcal{H}_o e^{-\frac{i}{\hbar}\mathcal{H}_o t} + \frac{i}{\hbar}e^{-\frac{i}{\hbar}\mathcal{H}_o t}\mathcal{H}_o A_s e^{-\frac{i}{\hbar}\mathcal{H}_o t} \\ &= -\frac{i}{\hbar}e^{\frac{i}{\hbar}\mathcal{H}_o t}A_s e^{-\frac{i}{\hbar}\mathcal{H}_o t}\mathcal{H}_o + \frac{i}{\hbar}\mathcal{H}_o e^{\frac{i}{\hbar}t}A_s e^{-\frac{i}{\hbar}\mathcal{H}_o t} \\ &= -\frac{i}{\hbar}A_I\mathcal{H}_o + \frac{i}{\hbar}\mathcal{H}_o A_I\end{aligned} \tag{A.26}$$

$$\frac{d}{dt}A_I = -\frac{i}{\hbar}[A_I, \mathcal{H}_o]. \tag{A.27}$$

So, taking our special case $\mathcal{H}_o = \hbar\omega_o b^\dagger b + \hbar\omega_1\hat{n}_1 + \hbar\omega_2\hat{n}_2$ and considering $A_s = \hat{b}$ then

$$\begin{aligned}\frac{d}{dt}\hat{b_I} &= -\frac{i}{\hbar}[\hat{b}_1\mathcal{H}_o] = -\frac{i}{\hbar}\hbar\omega_o[b_1, b^\dagger b] - \frac{i}{\hbar}\hbar\omega_1[b_1, \hat{n}_1] - \frac{i}{\hbar}\hbar\omega_2[b_1, \hat{n}_1] \\ &= -i\omega_o(b, b^\dagger b - b^\dagger bb) \\ &= -i\omega_o b\end{aligned} \tag{A.28}$$

So $b(t) = e^{(-i\omega_o t)}b(0)$.
We note that $b_s(0) = b_I(0)$ so where $b_s(b_I)$ is the atomic lowering operator in the Schrödinger (interaction) picture.

$$\begin{aligned}\hat{b}_I(t) &= e^{(-i\omega_o t)} \\ b_I(0) &= e^{(-i\omega_o t)}b_s\end{aligned} \tag{A.29}$$

Similarly,

$$\begin{aligned}a_{1I}(t) &= e^{(-i\omega_1 t)}a_{1s} \\ a_{2I}(t) &= e^{(-i\omega_2 t)}a_{2s},\end{aligned} \tag{A.30}$$

where again, the subscripts s and I refer to the Schrödinger and Interaction picture.
The interaction Hamiltonian in the Schrödinger picture is:

$$\mathcal{H}_{Is} = \hbar(g_1 b^\dagger a_1 + g_2 b^\dagger a_2 + g_1^\dagger a_1^\dagger b + g_2^\dagger a_2^\dagger b) \tag{A.31}$$

To get to the interaction picture we need to replace all operator above by the time-dependent

version

$$\begin{aligned}\mathcal{H}_{II} =&\hbar(g_1 e^{i\omega_o t} e^{-i\omega_1 t} b^\dagger a_1 + g_2 e^{i\omega_o t} e^{-i\omega_2 t} b^\dagger a_2 + \\ & g_1^\dagger e^{-i\omega_o t} e^{i\omega_1 t} a_1^\dagger b + g_2^\dagger e^{-i\omega_o t} e^{i\omega_2 t} a_2^\dagger b) \\ \mathcal{H}_{II} =&\hbar(g_1 b^\dagger a_1 e^{-i\delta_1 t} + g_2 b^\dagger a_2 e^{-i\delta_2 t} + g_1^\dagger a_1^\dagger b e^{i\delta_1 t} + g_2^\dagger a_2^\dagger b e^{i\delta_2 t}),\end{aligned} \tag{A.32}$$

where the H_{II} denotes the interaction Hamiltonian in the interaction picture.

From now on, we will write in the interaction picture exclusively. So we'll drop the distinction and simply write

$$\mathcal{H}_I = \hbar g_1 b^\dagger a_1 e^{-i\delta_1 t} + \hbar g_1^\dagger a_1^\dagger b e^{i\delta_1 t} + \hbar g_2 b^\dagger a_2 e^{i\delta_1 t} + \hbar g_2^\dagger a_2^\dagger b e^{i\delta_2 t}, \tag{A.33}$$

where δ_1 is the laser detuning from atomic resonance and δ_2 (δ_2 = ω_2-ω_0) is vacuum state detuning from atomic resonance.

A.2.1 Formulation of the L Matrix

With the interaction Hamiltonian in the interaction picture, we can come back to the Schrödinger equation A.23:

$$\frac{d}{dt}\psi_{int}(t) = \frac{-i}{\hbar}\mathcal{H}_{int}\psi_{int}(t) \tag{A.34}$$

In all our calculations, we will assume we start with the atom in the ground state, the pump initially has n photons and the vacuum mode has zero photons. Thus the initial state will always be $|g, n, 0\rangle$. To establish the pattern we are after, we will start with simple cases. Note here that with this notation n is not only the number of photons in the pump mode but also the number of excitations in the system. Starting with $n = 0$, let's apply try the Hamiltonian to the state $|g, 0, 0\rangle$ (which forms the right side of the Equation A.34):

$$\mathcal{H}_I\,|g, 0, 0\rangle = \hbar g_1 e^{-i\delta_1 t}\,|g, 0, 0\rangle = 0.$$

Nothing changes because with the atom is in the ground state and there are no photons in the system.

For $n = 1$, we apply the Hamiltonian to the possible states $|g, 0, 0\rangle$, $|g, 0, 0\rangle$ and $|g, 0, 0\rangle$:

$$
\begin{aligned}
\mathcal{H}_I \left|g,1,0\right\rangle &= \hbar g_1 e^{-i\delta_1 t} \left|e,0,0\right\rangle \\
\mathcal{H}_I \left|e,0,0\right\rangle &= \hbar g_1^\dagger e^{i\delta_1 t} \left|g,1,0\right\rangle + \hbar g_2^\dagger e^{i\delta_2 t} \left|g,0,1\right\rangle \\
\mathcal{H}_I \left|g,0,1\right\rangle &= \hbar g_2 e^{-i\delta_2 t} \left|e,0,0\right\rangle .
\end{aligned}
$$

Since $\frac{d}{dt}\psi = L\psi$ and if we define $\psi = \begin{bmatrix} |g,1,0\rangle \\ |e,0,0\rangle \\ |g,0,1\rangle \end{bmatrix}$ then, the Equation A.34 can be written as

$$
\frac{d}{dt}\begin{bmatrix} |g,1,0\rangle \\ |e,0,0\rangle \\ |g,0,1\rangle \end{bmatrix} = -\frac{i}{\hbar}\begin{bmatrix} 0 & \hbar g_1 e^{-i\delta_1 t} & 0 \\ \hbar g_1^\dagger e^{i\delta_1 t} & 0 & \hbar g_2^\dagger e^{i\delta_2 t} \\ 0 & \hbar g_2^\dagger e^{i\delta_2 t} & 0 \end{bmatrix}\begin{bmatrix} |g,1,0\rangle \\ |e,0,0\rangle \\ |g,0,1\rangle \end{bmatrix}. \tag{A.35}
$$

If we define L by the matrix L = $\begin{bmatrix} 0 & 1 & 0 \\ 1 & 0 & 1 \\ 0 & 1 & 0 \end{bmatrix}$, then we have $\frac{d}{dt}\psi = L\psi$.

Similarly, for $n = 2$, $\psi = \begin{bmatrix} |g,2,0\rangle \\ |e,1,0\rangle \\ |g,1,1\rangle \\ |e,0,1\rangle \\ |g,0,2\rangle \end{bmatrix}$, we apply the Hamiltonian on all states:

$$
\begin{aligned}
\mathcal{H}_I \left|g,2,0\right\rangle &= \hbar g_1 \sqrt{2} e^{-i\delta_1 t} \left|e,1,0\right\rangle \\
\mathcal{H}_I \left|e,1,0\right\rangle &= \hbar g_1^\dagger \sqrt{2} e^{i\delta_1 t} \left|g,2,0\right\rangle + \hbar g_2^\dagger e^{i\delta_2 t} \left|g,1,1\right\rangle \\
\mathcal{H}_I \left|g,1,1\right\rangle &= \hbar g_1 e^{-i\delta_1 t} \left|e,0,1\right\rangle + \hbar g_2 e^{-i\delta_2 t} \left|e,1,0\right\rangle \\
\mathcal{H}_I \left|e,0,1\right\rangle &= \hbar g_1^\dagger e^{i\delta_1 t} \left|g,1,1\right\rangle + \hbar g_2^\dagger \sqrt{2} e^{i\delta_2 t} \left|g,0,2\right\rangle \\
\mathcal{H}_I \left|g,0,2\right\rangle &= \hbar g_2 \sqrt{2} e^{-i\delta_2 t} \left|e,0,1\right\rangle
\end{aligned}
$$

Without the coupling constants and exponential parts, $\mathrm{L} = \begin{bmatrix} 0 & \sqrt{2} & 0 & 0 & 0 \\ \sqrt{2} & 0 & 1 & 0 & 0 \\ 0 & 1 & 0 & 1 & 0 \\ 0 & 0 & 1 & 0 & \sqrt{2} \\ 0 & 0 & 0 & \sqrt{2} & 0 \end{bmatrix}$.

For $n = 3$, $\psi = \begin{bmatrix} |g,3,0\rangle \\ |e,2,0\rangle \\ |g,2,1\rangle \\ |e,1,1\rangle \\ |g,1,2\rangle \\ |e,0,2\rangle \\ |g,0,3\rangle \end{bmatrix}$, we apply the Hamiltonian on all states:

$$
\begin{aligned}
\mathcal{H}_I\,|g,3,0\rangle &= \hbar g_1 \sqrt{3} e^{-i\delta_1 t}\,|e,2,0\rangle \\
\mathcal{H}_I\,|e,2,0\rangle &= \hbar g_1^\dagger \sqrt{3} e^{i\delta_1 t}\,|g,3,0\rangle + \hbar g_2^\dagger e^{i\delta_2 t}(1)\,|g,2,1\rangle \\
\mathcal{H}_I\,|g,2,1\rangle &= \hbar g_1 e^{-i\delta_1 t}\sqrt{2}\,|e,1,0\rangle + \hbar g_2 e^{-i\delta_2 t}(1)\,|e,2,0\rangle \\
\mathcal{H}_I\,|e,1,1\rangle &= \hbar g_1^\dagger e^{i\delta_1 t}\sqrt{2}\,|g,2,0\rangle + \hbar g_2^\dagger \sqrt{2} e^{i\delta_2 t}\,|g,1,2\rangle \\
\mathcal{H}_I\,|g,1,2\rangle &= \hbar g_1^\dagger e^{i\delta_1 t}\,|e,0,2\rangle + \hbar g_2 e^{-i\delta_2 t}\sqrt{2}\,|e,1,1\rangle \\
\mathcal{H}_I\,|e,0,2\rangle &= \hbar g_1^\dagger e^{i\delta_1 t}(1)\,|g,1,2\rangle + \hbar g_2^\dagger e^{i\delta_2 t}\sqrt{3}\,|g,0,3\rangle \\
\mathcal{H}_I\,|g,0,3\rangle &= \hbar g_2 e^{-i\delta_1 t}\sqrt{3}\,|e,0,2\rangle
\end{aligned}
$$

Without the coupling constants and exponential parts, the matrix L becomes

$$
L = \begin{bmatrix} 0 & \sqrt{3} & 0 & 0 & 0 & 0 & 0 \\ \sqrt{3} & 0 & 1 & 0 & 0 & 0 & 0 \\ 0 & 1 & 0 & \sqrt{2} & 0 & 0 & 0 \\ 0 & 0 & \sqrt{2} & 0 & \sqrt{2} & 0 & 0 \\ 0 & 0 & 0 & \sqrt{2} & 0 & 1 & 0 \\ 0 & 0 & 0 & 0 & 1 & 0 & \sqrt{3} \\ 0 & 0 & 0 & 0 & 0 & \sqrt{3} & 0 \end{bmatrix}.
$$

For $n = 4$, $\psi = \begin{bmatrix} |g,4,0\rangle \\ |e,3,0\rangle \\ |g,3,1\rangle \\ |e,2,1\rangle \\ |g,2,2\rangle \\ |e,1,2\rangle \\ |g,1,3\rangle \\ |e,0,3\rangle \\ |g,0,4\rangle \end{bmatrix}$, we apply the Hamiltonian on all states:

$$
\begin{aligned}
\mathcal{H}_I\,|g,4,0\rangle &= \hbar g_1\sqrt{4}e^{-i\delta_1 t}\,|e,3,0\rangle \\
\mathcal{H}_I\,|e,3,0\rangle &= \hbar g_1^\dagger\sqrt{4}e^{i\delta_1 t}\,|g,4,0\rangle + \hbar g_1^\dagger e^{i\delta_2 t}(1)\,|g,3,1\rangle \\
\mathcal{H}_I\,|g,3,1\rangle &= \hbar g_1\sqrt{3}e^{-i\delta_1 t}\,|e,2,1\rangle + \hbar g_2(1)e^{-i\delta_2 t}\,|e,3,0\rangle \\
\mathcal{H}_I\,|e,2,1\rangle &= \hbar g_1^\dagger\sqrt{3}e^{i\delta_1 t}\,|g,3,1\rangle + \hbar g_2^\dagger\sqrt{2}e^{i\delta_2 t}\,|g,2,2\rangle \\
\mathcal{H}_I\,|g,2,2\rangle &= \hbar g_1^\dagger\sqrt{2}e^{-i\delta_1 t}\,|e,1,2\rangle + \hbar g_2\sqrt{2}e^{-i\delta_2 t}\,|e,2,1\rangle \\
\mathcal{H}_I\,|e,1,2\rangle &= \hbar g_1^\dagger\sqrt{2}e^{i\delta_1 t}(1)\,|g,2,2\rangle + \hbar g_2^\dagger\sqrt{3}e^{i\delta_2 t}\,|g,1,3\rangle \\
\mathcal{H}_I\,|g,1,3\rangle &= \hbar g_1\sqrt{1}e^{-i\delta_1 t}\,|e,0,3\rangle + \hbar g_2\sqrt{3}e^{-i\delta_2 t}\,|e,1,2\rangle \\
\mathcal{H}_I\,|e,0,3\rangle &= \hbar g_1^\dagger\sqrt{1}e^{i\delta_1 t}\,|g,1,3\rangle + \hbar g_2^\dagger\sqrt{4}e^{i\delta_2 t}\,|g,0,4\rangle \\
\mathcal{H}_I\,|g,0,4\rangle &= \hbar g_2\sqrt{4}e^{i\delta_2 t}\,|e,0,3\rangle
\end{aligned}
$$

Preparing the L matrix (without the coupling constants and exponential parts):

$$
L = \begin{bmatrix}
0 & \sqrt{4} & 0 & 0 & 0 & 0 & 0 & 0 & 0 \\
\sqrt{4} & 0 & 1 & 0 & 0 & 0 & 0 & 0 & 0 \\
0 & 1 & 0 & \sqrt{3} & 0 & 0 & 0 & 0 & 0 \\
0 & 0 & \sqrt{3} & 0 & \sqrt{2} & 0 & 0 & 0 & 0 \\
0 & 0 & 0 & \sqrt{2} & 0 & \sqrt{2} & 0 & 0 & 0 \\
0 & 0 & 0 & 0 & \sqrt{2} & 0 & \sqrt{3} & 0 & 0 \\
0 & 0 & 0 & 0 & 0 & \sqrt{3} & 0 & 1 & 0 \\
0 & 0 & 0 & 0 & 0 & 0 & 1 & 0 & \sqrt{4} \\
0 & 0 & 0 & 0 & 0 & 0 & 0 & \sqrt{4} & 0
\end{bmatrix}
$$

Now, that we went over the L matrices for n = 1, 2, 3 and 4, we can see a pattern emerging. The L matrix is square size $(2n + 1) \cdot (2n + 1)$. Observing for example, the $n = 4$, the L matrix has four 3x3 matrices aligned along its diagonal of size 9.

Each 3x3 matrix exhibits the pattern: $\begin{bmatrix} 0 & \sqrt{a} & 0 \\ \sqrt{a} & 0 & \sqrt{b} \\ 0 & \sqrt{b} & 0 \end{bmatrix}$ where a + b = n+1.

The first 3x3 matrix , which is centered on row 2 and b = 1 and a = n + 1 - b = 4 looks like:

$$L = \begin{bmatrix} 0 & \sqrt{4} & 0 \\ \sqrt{4} & 0 & 1 \\ 0 & 1 & 0 \end{bmatrix}.$$

The next matrix in our example, is centered on row 4, b = 2 and a = 3 is $\begin{bmatrix} 0 & \sqrt{3} & 0 \\ \sqrt{3} & 0 & \sqrt{2} \\ 0 & \sqrt{2} & 0 \end{bmatrix}$.

The third matrix, centered on row 4 has b = 3 and a = 2 is $\begin{bmatrix} 0 & \sqrt{2} & 0 \\ \sqrt{2} & 0 & \sqrt{3} \\ 0 & \sqrt{3} & 0 \end{bmatrix}$.

The forth matrix and last matrix in our example is centered on row 6 has b = 4 and a = 1 is

$$\begin{bmatrix} 0 & 1 & 0 \\ 1 & 0 & \sqrt{4} \\ 0 & \sqrt{4} & 0 \end{bmatrix}.$$

Now, we have to add the coupling constants and exponential parts to the L matrix, that also follows an observable pattern .

Finally we get to the point to where we can calculate the number of photons that moves from the pump beam to the probe beam and it is detected by the photodetector.

For $n = 4$, we have:

$$
\begin{aligned}
|\psi\rangle &= C_1\,|g,4,0\rangle + C_2\,|e,3,0\rangle + C_3\,|g,3,1\rangle + C_4\,|e,2,1\rangle + C_5\,|g,2,2\rangle + \\
&\quad C_6\,|e,1,2\rangle + C_7\,|g13\rangle + C_8\,|e,3,0\rangle + C_9\,|g,0,4\rangle \\
\langle\psi|\,n_1\,|\psi\rangle &= 4|C_1|^2 + 3|C_2|^2 + 3|C_3|^2 + 2|C_4|^2 + 2|C_5|^2 + |C_6|^2 + |C_7|^2 \\
\langle\psi|\,n_2\,|\psi\rangle &= |C_3|^2 + |C_4|^2 + 2|C_5|^2 + |C_6|^2 + 3|C_7|^2 + 3|C_8|^2 + 4|C_9|^2
\end{aligned}
$$

We are also interested in $\langle a_2^\dagger a_1\rangle = \langle a_1^\dagger a_2\rangle$, which is a measure of noise amplitude.

$$
\begin{aligned}
a_1\,|\psi\rangle &= \sqrt{4}\,C_1\,|g,3,0\rangle + \sqrt{3}\,C_2\,|e,2,0\rangle + \sqrt{3}\,C_3\,|g,2,1\rangle + \sqrt{2}\,C_4\,|e,1,1\rangle + \\
&\quad \sqrt{2}\,C_5\,|g,1,2\rangle\,\sqrt{1}\,C_6\;\;|e,0,2\rangle + \sqrt{1}\,C_7\,|g,0,3\rangle \\
a_2^\dagger a_1\,|\psi\rangle &= \sqrt{1}\,4\,C_1\,|g,3,1\rangle + \sqrt{3}\,1\,C_2\,|e,2,1\rangle + \sqrt{3}\sqrt{2}\,C_3\,|g,2,2\rangle + \sqrt{2}\sqrt{2}\,C_4\,|e,1,2\rangle + \\
&\quad \sqrt{2}\sqrt{3}\,C_5\,|g,1,3\rangle + \sqrt{1}\sqrt{3}\,C_6\,|g,1,3\rangle + \sqrt{1}\sqrt{4}\,C_7\,|g,0,4\rangle \\
\langle\psi|\,a_2^\dagger a_1\,|\psi\rangle &= \sqrt{1}\,\sqrt{4}\,C_3^*C_1 + \sqrt{1}\,\sqrt{3}\,C_4^*C_2 + \sqrt{2}\sqrt{3}\,C_5^*C_3 + \sqrt{2}\sqrt{2}\,C_6^*C_4 + \\
&\quad \sqrt{3}\sqrt{2}\,C_7^*C_5 + \sqrt{3}\sqrt{1}\,C_8^*C_6 + \sqrt{1}\sqrt{4}\,C_9^*C_7
\end{aligned}
$$

$$
\begin{aligned}
a_2\,|\psi\rangle &= \sqrt{1}\,C_3\,|g,3,0\rangle + \sqrt{1}\,C_4\,|e,2,0\rangle + \sqrt{2}\,C_5\,|g,2,1\rangle + \sqrt{2}\,C_6\,|e,1,1\rangle + \\
&\quad \sqrt{3}\,C_7\,|g,1,2\rangle + \sqrt{3}\,C_8\;\;|e,0,2\rangle + \sqrt{4}\,C_9\,|g,0,3\rangle \\
a_1^\dagger a_2\,|\psi\rangle &= \sqrt{1}\sqrt{4}\,C_3\,|g,4,0\rangle + \sqrt{1}\sqrt{3}\,C_4\,|e,3,0\rangle + \sqrt{2}\sqrt{3}\,C_5\,|g,2,2\rangle + \sqrt{2}\sqrt{2}\,C_4\,|e,1,2\rangle + \\
&\quad \sqrt{2}\sqrt{3}\,C_5\,|g,1,3\rangle + \sqrt{1}\sqrt{3}\,C_6\,|g,1,3\rangle + \sqrt{1}\sqrt{4}\,C_7\,|g,0,4\rangle \\
\langle\psi|\,a_1^\dagger a_2\,|\psi\rangle &= \sqrt{1}\,\sqrt{4}\,C_1^*C_4 + \sqrt{1}\,\sqrt{3}\,C_2^*C_4 + \sqrt{2}\sqrt{3}\,C_3^*C_5 + \sqrt{2}\sqrt{2}\,C_4^*C_6 + \\
&\quad \sqrt{3}\sqrt{2}\,C_5^*C_7 + \sqrt{3}\sqrt{1}\,C_6^*C_8 + \sqrt{4}\sqrt{1}\,C_7^*C_9
\end{aligned}
$$

We have than verified that $\langle\psi|a_2^\dagger a_1|\psi\rangle$ is equal to $\langle\psi|a_1^\dagger a_2|\psi\rangle$.

From the equations above we can construct the following equations:

$$
\langle n_1\rangle^2 = \sum_{n=2}^{2N}(N - \frac{1}{2}n)|C_n|^2 + \sum_{n=1}^{2N+1}\frac{1}{2}(2N + 1 - n)|C_n|^2
$$

$$\langle n_2 \rangle^2 = \sum_{n=2}^{2N} (\frac{1}{2}n - 1)|C_n|^2 + \sum_{n=1}^{2N+1} \frac{1}{2}(n-1)|C_n|^2$$

$$\langle a_2^\dagger a_1 \rangle = \sum_{n=2}^{2N-1} \sqrt{(N - \frac{1}{2}n)}\sqrt{(\frac{1}{2}n)}\, C_{N+2}^*\, C_n + \sum_{n=1}^{2N-1} \sqrt{\frac{1}{2}(n+1)}\sqrt{\frac{1}{2}(2N+1-n)}\, C_{N+2}^*\, C_n.$$

Where the first part of equation A.2.1 is the summation of terms for even n integers and the second part is the summation of terms for n odd integers.

A.3 MATLAB Code for Excess Noise in Function of Laser Intensity (based on theoretical derivation)

```
%
%  ExcessNoisev4
%
%  This version puts the correct square root coefficient into the matrix
%  and also accounts for detuning
%
%  Note:
%     1.The way the equations are constructed here, numPh is the number
%       of photons in the initial pump state AND the total number of
%       excitations (since the atom starts in the ground state)
%     2. Detuning is not included here. The solution Psi=exp(Lt)Psi0 is
%     not valid when L is time dependent.
%     3. Added saving the time series and fft plots.
%
%  Additional note; Go to ExcessNoisev3 for solutions via ODE45, so that
%  detuning is properly handled.
%
%  Notes for version 3:
%     1. Rewrote the integration part to use ODE45
%
%  Notes for version 4:
%     1. Rewrote the probability calculation part to match notation of
%     notes from 10/24
%     2. Now include number of photons in pump mode
%

%function [y,z]=ExcessNoise(del1)
%clear vars -except numPh
%clear variables;
%close all;
%global numPh
%clc;
%numPh
x1=.0;     % left edge relative to left side of monitor on scale of 0 to 1.
y1=.15;     % bottom edge relative to monitor bottom going up on scale of 0 to 1.
Dx=.35;     % width of figure
Dy=.55;     % height of figure


%numPh=input('Enter number of photons initially in the pump state ==> ');
numPh=10;
```

```
%tmax=input('Enter tmax in units of pi ===> ');
%mpts=input('Enter number of time points ===> ');;    %number of time points
%mpts=1000;   %Number of time points
tmax=250;
tmax=tmax*pi;
%tic;
iFFT=1;     %Set =1 if desire to take FFT of photon number at end.
isave=0;    %Set=1 to save graphs
iplot1=0;   %Plot atomic variables
iplot2=0;   %Plot field
iplot3=0;   %Plot FFT

%
%   Create L
%
L=zeros(2*numPh+1,2*numPh+1);
%   Populate
disp(['In routine del1 ' ' ' num2str(del1)])
del2=1;
g1=1+0*1i;;
g2=1+0*1i;

Psi0=zeros(2*numPh+1,1);
Psi0(1)=1;
% Psi=zeros(mpts,2*numPh+1);
%tic

options=odeset('RelTol',1e-6,'AbsTol',1e-6);
tspan=[0 tmax];
[t,Psi]=ode45('ExcessNoisev3_sub',tspan,Psi0,options,numPh,g1,g2,del1,del2);

%toc

%
%   Atomic population plots
%
cd ('FFT Plots')
Prob_gnd=zeros(size(t));
Prob_ex=zeros(size(t));
for n=2:2:2*numPh
   Prob_ex(:)=Prob_ex(:)+Psi(:,n).*conj(Psi(:,n));
```

```
end
for n=1:2:2*numPh+1
   Prob_gnd(:)=Prob_gnd(:)+Psi(:,n).*conj(Psi(:,n));
end
if iplot1
   fid2=figure('units','normalized','outerposition',[x1+.32 y1 Dx Dy]);
   plot(t/pi,Prob_gnd,t/pi,Prob_ex,t/pi,Prob_gnd+Prob_ex);
   xlabel('time/$\pi$')
   legend('Gnd','Exc','Sum')
end
%
% %Number of photons in pump mode vs time
%
Prob_p=zeros(size(t));
for n=2:2:2*numPh
   Prob_p(:)=Prob_p(:)+(numPh-0.5*n)*Psi(:,n).*conj(Psi(:,n));
end
for n=1:2:2*numPh+1
   Prob_p(:)=Prob_p(:)+0.5*(2*numPh+1-n)*Psi(:,n).*conj(Psi(:,n));
end
tol=1e-6;
if max(imag(Prob_p))>=tol
   disp('Problem=Prob is complex!!!')
end

% %
% %Number of photons in vacuum mode vs time
%

Prob_n=zeros(size(t));
for n=2:2:2*numPh
   Prob_n(:)=Prob_n(:)+(0.5*n-1)*Psi(:,n).*conj(Psi(:,n));
end
for n=1:2:2*numPh+1
   Prob_n(:)=Prob_n(:)+0.5*(n-1)*Psi(:,n).*conj(Psi(:,n));
end
tol=1e-6;
if max(imag(Prob_n))>=tol
   disp('Problem=Prob is complex!!!')
end
if iplot2
```

```
    fid3=figure('units','normalized','outerposition',[x1+.68 y1 Dx Dy]);
    plot(t/pi,real(Prob_p),t/pi,real(Prob_n),t/pi,real(Prob_n+Prob_p+Prob_ex));%,t,
0.25*(cos(sqrt(2)*t).*cos(sqrt(2)*t)-2*cos(sqrt(2)*t)+1))
    xlabel('time/$\pi$')
    legend('Pump Photon No. ','Vac photon No','Total Photon No.')
    if isave
        FileName=strcat('Time Series N=',num2str(numPh));
        set(fid3,'PaperOrientation','landscape');
        print(FileName,'-dpdf','-bestfit')
        saveas(gcf,FileName,'fig')
        set(fid3,'PaperOrientation','portrait');
        saveas(gcf,FileName,'jpg')
    end
end
mpts=length(t);
f=[-mpts/2:1:mpts/2-1]/tmax;
F=fftshift(fft(Prob_n-mean(Prob_n)));
if iplot3
    fid4=figure('units','normalized','outerposition',[x1+.15 y1 Dx Dy]);
    plot(2*pi*f,F.*conj(F)/max(F.*conj(F)))
    v=axis;
    axis([v(1) v(2) 0 1.5])
    xlabel('Freq ($\nu$)')
    if isave
        FileName=strcat('Fourier Series N=',num2str(numPh));
        set(fid4,'PaperOrientation','landscape');
        print(FileName,'-dpdf','-bestfit')
        saveas(gcf,FileName,'fig')
        set(fid4,'PaperOrientation','portrait');
        saveas(gcf,FileName,'jpg')
    end
end
cd ..
hold on
% y=Prob_n;
% z=Prob_ex;
%end
```

A.4 MATLAB Code for Excess Noise in Function of Laser Intensity (based on experimental data)

```
%  ReadIt_14JulV2
%
%  Program to analyze the data take on Jul 14, 2020.
%  Program reads the data file exported from the spectrum analyzer

% From the paper:
% "Excess noise acquired by a laser beam after propagating through an%
atomic-potassium vapor.pdf"
%
%   Version 2:
%       This code does exactly what ReadIt_13Jul does except that reading
%       the multiple files is done in a loops (with comments).

%%
clear variables     %makes sure no remenants from previous runs are left
close all           %close all plot screens
clc;                %clear command line
%
%   Program constants
%
x1=.2;      % left edge relative to left side of monitor on scale of 0 to 1.
y1=.1;      % bottom edge relative to monitor bottom going up on scale of 0
to 1.
Dx=.55;     % width of figure
Dy=.85;     % height of figure

mycolor(1:3)=[1,0,0];           %red
mycolor(4:6)=[0,0,1];           %blue
mycolor(7:9)=[0,1,0];           %green
mycolor(10:12)=[0,0,0];         %black
%
%   Numbers specific to this day's data runs
%
F=[1,2,3,4];                            %possible values of scan frequency
Flabel=[0.5,1,5,10];
P=[0,15,36,97];                         %possible values of laser power

%
%   Begin the plotting of traces versus temperature

for m=1:length(F)
    fileList=dir(strcat('*F=',num2str(F(m)),'*.DAT'));          %find all
files with T=65 in the name
    % and put it in the structure fileList
    numFiles=length(fileList);                                  %stores the
number of files in numFiles
    if (numFiles==0)                                            %the file with
65 doesn't have a V in it
        fileList=dir(strcat('*F=',num2str(F(m)),'*.DAT'));      %find all
files with T=65 in the name
        % and put it in the structure fileList
        numFiles=length(fileList);                              %stores the
number of files in numFiles
    end
    fid=figure('name',strcat('Frequency =
```

```
',num2str(Flabel(m))),'units','normalized','outerposition',[x1 y1 Dx Dy]);
    for n=1:numFiles
        A=dlmread(fileList(n).name,';',29,0);
%First value of frequency not written correctly in file
        xdata=A(:,1);
        ydata=A(:,2);
        plot(xdata,ydata,'color',mycolor(3*n-2:3*n),'linewidth',1.1);
        xt = get(gca, 'XTick');
        set(gca, 'FontSize', 16);
        xlabel('Frequency');
        ylabel('dBm');
        title(strcat('Frequency = ',num2str(Flabel(m)),' MHz'))
        hold on
    end
    legend('no light','0.15mW','0.36mW','0.97mW')
%    legend(fileList.name) %delete or comment out when done checking file
name
    xlim([0 0.1])
    ylim([-85 -50])
    pause(1);
end
%%
disp('about to do next section-')
pause;
%*****************************

for m=1:length(P)
    fileList=dir(strcat('*',num2str(P(m)),'T*.DAT'));       % find all files
with T=65 in the name
                                                            % and put it in
the structure fileList
    numFiles=length(fileList);                              % stores the
number of files in numFiles
    if (numFiles==0)                                        % the file with
65 doesn't have a V in it
        fileList=dir(strcat('*',num2str(P(m)),'T*.DAT'));   % find all files
with T=65 in the name
        % and put it in the structure fileList
        numFiles=length(fileList);                          %stores the
number of files in numFiles
    end

    fid=figure('name',strcat('Power =
',num2str(P(m))),'units','normalized','outerposition',[x1 y1 Dx Dy]);
    for n=1:numFiles
        A=dlmread(fileList(n).name,';',29,0);                %First value of
frequency not written correctly in file
        xdata=A(:,1);
        ydata=A(:,2);
        plot(xdata,ydata,'color',mycolor(3*n-2:3*n),'linewidth',1.1);
        xt = get(gca, 'XTick');
        set(gca, 'FontSize', 16);
        xlabel('Frequency');
        ylabel('dBm');
        title(strcat('Power = ',num2str(P(m)),' mWatts'))
```

```
        hold on
    end
    legend(strcat('F=',num2str(Flabel(1)),'
MHz'),strcat('F=',num2str(Flabel(2)),' MHz'),...
           strcat('F=',num2str(Flabel(3)),'
MHz'),strcat('F=',num2str(Flabel(4)),' MHz'))
%   legend(fileList.name)  %delete or comment out when done checking file
name

    xlim([0 0.1])
    ylim([-85 -50])
end
```

A.5 MATLAB Code for Raw Data Transfer from Oscilloscope for Plotting

```
%   ReadfromScopev2.m
%
%   Written by: Dr. Frank A. Narducci
%   Written on: October 10, 2017
%   Modified by: Renata
%
%   This program reads data files stored by the oscilloscope in their csv format.
%
%   Version 2: Used to simply read the data file

clear all; close all;

[fileName,pathName] = uigetfile('*.*','Enter file to be read');
cd(pathName);
% create a matrix with all the numbers that we can use to plot. The numbers
% in this case they start from line 17. Everything above line 16 is not copied.
A = dlmread(strcat(pathName,fileName),',',16,0);
d = size(A);
disp(strcat('The number of columns is = ',num2str(d(2))));
disp('I will assume the x-axis will come from column 1');
iplot = input('Enter columns you wish to plot (in [1 2 3] format ==> ');

for n=1:length(iplot)
    fid(n)=figure;
    plot(A(:,1),A(:,iplot(n)))

    if n==1
        set(fid(1),'Position',[10 565 630 430])
    elseif n==2
        set(fid(2),'Position',[655 565 630 430])
    elseif n==3
        set(fid(3),'Position',[1300 565 630 430])
    elseif n==4
        set(fid(4),'Position',[10 50 630 430])
    elseif n==5
        set(fid(5),'Position',[655 50 630 430])
    elseif n==6
        set(fid(6),'Position',[1300 50 630 430])
    end
end
pause;

close all
fid=figure('units','normalized','outerposition',[0 0 1 1]);
plot(A(:,1)*1000,A(:,4),'LineWidth',3);
v=axis;
axis([min(A(:,1)*1000) max(A(:,1)*1000) v(3) v(4)])
xt = get(gca, 'XTick');
set(gca, 'FontSize', 16)%This must be executed first or it
%overwrites other label commands
xlabel('Freq. (arb. units)','Interpreter','LaTex', 'Fontsize',26)
ylabel('Sat. Abs. (arb. units)','Interpreter','LaTex', 'Fontsize',26)

yyaxis right
nbox=50;
for i=1:length(A)-nbox
    x_ave(i)=mean(A(i:i+nbox,1));
    y_ave(i)=mean(A(i:i+nbox,3));
end
```

```
plot(A(:,1)*1000,-A(:,3),'or',x_ave*1000,-y_ave,'-k','LineWidth',3);
%plot(A(:,1)*1000,-A(:,3),'r','LineWidth',3);
ylabel('Fluorescence','Interpreter','LaTex', 'Fontsize',26)

title(strcat(pathName,fileName),'Interpreter','LaTeX','Fontsize',30)
cd
%set(fid,'Position',[1 41 1920 964])
set(fid,'PaperOrientation','landscape');
print(fileNameshort,'-dpdf','-bestfit')
saveas(gcf,fileNameshort,'fig')
set(fid,'PaperOrientation','portrait');
saveas(gcf,fileNameshort,'jpg')

%   Positions for 6 windows
%[ num, txt, raw ]   = xlsread( strcat(pathName,fileName) );

function Str = FirstUpper(Str)
% Upper case of first letter, lower case for rest
% UStr = FirstUpper(Str)
% Input string can be a cell string.
%
% Tested: Matlab 6.5, 7.7, 7.8, 7.13, WinXP/32, Win7/64
% Author: Jan Simon, Heidelberg, (C) 2007-2011 matlab.THISYEAR(a)n-simonDOTde

if isempty(Str)
    return;
end

if ischar(Str)
    Str    = lower(Str);
    Str(1) = upper(Str(1));
else  % Cell string, hopefully:
    % Do the work on each cell entry:
    Str = lower(Str);
    for iC = 1:numel(Str)
        thisStr = Str{iC};
        lenStr  = length(thisStr);
        if lenStr == 1
            Str{iC} = upper(thisStr);
        elseif lenStr  % > 1: Change just the first character:
            Str{iC}(1) = upper(thisStr(1));
        end %if lenStr
    end %for iC
end %ischar(Str)
end
```

```
%   DataFit.m
%
%   Written by: Dr. Frank A. Narducci
%   Written on: February 10, 2007
%
%  This program was canabilized from SampleDataFit.m
%
%   It is designed to fit the two curves in Tek0 of this data file
%   to Gaussian functions and measur ethe shift between them.

clear variable;
close all;
```

```
%   Read the data

[fileName,pathName]=uigetfile('*.csv','Pick the data file');
A=dlmread(fileName,',',16,0);
tdata=A(:,1);
ydata=A(:,2);

%   Now try to fit the data
%
npts=length(ydata);
[A0,in]=max(ydata);          %Initial guess for amplitude and its index
t0=tdata(in);                %Initial guess for t0
for n=in:npts                   %Find the HWHM
    if (ydata(n)>=0.5*A0) continue
    else
        break
    end
end
tau=0.1*abs(tdata(n));       %initial guess for tau
offset=0;                    %Initial guess for offset
p=[A0,t0,tau,offset];

options=optimset('Display','off');
%Turns off the termination condition output

p_best=lsqcurvefit(@myfun,p,tdata,ydata,[],[],options);
%Empty matrices are lower and upper bounds for p

ytheory=myfun(p_best,tdata);
%   Plot the results
%
fid=figure;
plot(tdata,ydata,'*b',tdata,ytheory,'r');
pause;
close(fid);
```

```
%   MyFun.m
%
%   Sample function
%
function y=myfun(p,t)
%
%   From the program we have:
%   p=[A0,t0,tau,offset];
%
A0=p(1);
t0=p(2);
tau=p(3);
offset=p(4);
y=A0*exp(-(t-t0).*(t-t0)/(tau*tau))+offset;
```

List of References

[1] Log - nautical instrument. (2004, Apr. 29). Encyclopaedia Britannica. [Online]. Available: https://www.britannica.com/technology/log-nautical-instrument

[2] M. Denny. (2012). *The Science of Navigation : From Dead Reckoning to GPS*. Johns Hopkins University Press. [Online]. Available: https://ebookcentral.proquest.com/lib/ebook-nps/detail.action?docID=3318705

[3] D. Sobel, *Longitude : The True Story of a Lone Genius Who Solved the Greatest Scientific Problem of His Time*, 17th ed. New York: Walker, 1995.

[4] S. Casey, *Set Phasers on Stun and Others True Tales of Design, Technology, and Human Error*, 2nd ed. Santa Barbara, CA: Aegean Publishing Company, 1993.

[5] Satellite Navigation - Risks to the System. (n.d.). Smithsonian National Air and Space Museum. [Online]. Available: https://timeandnavigation.si.edu/satellite-navigation/gps/risks-to-system. Accessed Oct. 6, 2020.

[6] R. D. Christ and R. L. Wernli. (2014). *ROV Manual - A User Guide for Remotely Operated Vehicles*. [Knovel Mechanics & Mechanical Engineering Academic]. [Online]. Available: https://app.knovel.com/hotlink/toc/id:kpROVMAU03/rov-manual-user-guide/rov-manual-user-guide

[7] K. Yu. (2018). *Positioning and Navigation in Complex Environments*. [IGI Global version]. [Online]. Available: https://www.igi-global.com/gateway/book/181077

[8] W. W. Chow, J. Gea-Banacloche, L. M. Pedrotti, V. E. Sanders, W. Schleich, and M. O. Scully, "The ring laser gyro," *Rev. Mod. Phys.*, vol. 57, pp. 61–104, Jan 1985. Available: https://link.aps.org/doi/10.1103/RevModPhys.57.61

[9] E. Hecht, *Optics*, 4th ed. San Francisco: Addison - Wesley, 2002.

[10] V. M. N. Passaro, A. Cuccovillo, L. Vaiani, M. De Carlo, and C. E. Campanella, "Gyroscope technology and applications: A review in the industrial perspective," *Sensors (Basel, Switzerland)*, vol. 17, pp. 2284–, 2017. Available: https://doi.org/10.3390/s17102284

[11] K. Cregge. (2017, Dec. 13). Automated Celestial Navigation for the Navy. *Maritime Executive*. [Online]. Available: https://www.maritime-executive.com/blog/automated-celestial-navigation-for-the-navy

[12] M. Smith. (2016, Sep. 16). Navy resumes teaching celestial navigation just in case GPS is neutralized – Update. [Online]. Available: https://spacepolicyonline.com/news/navy-resumes-teaching-celestial-navigation-just-in-case-gps-is-neutralized/

[13] G. T. Schmidt. (2015, Feb). Navigation sensors and systems in GNSS degraded and denied environments. *Chinese Journal of Aeronautics*. [Online]. *28*(1). Available: https://www.sciencedirect.com/science/article/pii/S1000936114002003

[14] A. Miffre, M. Jacquey, M. Büchner, G. Trénec, and J. Vigué, "Atom interferometry," *Physica Scripta*, vol. 74, no. 2, pp. C15–C23, Jul 2006. Available: https://doi.org/10.1088/0031-8949/74/2/N01

[15] O. Carnal and J. Mlynek, "Young's double-slit experiment with atoms: A simple atom interferometer," *Phys. Rev. Lett.*, vol. 66, pp. 2689–2692, May 1991. Available: https://link.aps.org/doi/10.1103/PhysRevLett.66.2689

[16] F. Riehle, T. Kisters, A. Witte, J. Helmcke, and C. J. Borde, "Optical ramsey spectroscopy in a rotating frame: Sagnac effect in a matter-wave interferometer," *Phys. Rev. Lett.*, vol. 67, pp. 177–180, Jul 1991. Available: https://link.aps.org/doi/10.1103/PhysRevLett.67.177

[17] K. Bongs, M. Holynski, J. Vovrosh, and et al., "Taking atom interferometric quantum sensors from the laboratory to real-world applications," *Nature Reviews Physics*, vol. 1, no. 12, Oct 2019. Available: https://doi.org/10.1038/s42254-019-0117-4

[18] D. W. Keith, C. R. Ekstrom, Q. A. Turchette, and D. E. Pritchard, "An interferometer for atoms," *Phys. Rev. Lett.*, vol. 66, pp. 2693–2696, May 1991. Available: https://link.aps.org/doi/10.1103/PhysRevLett.66.2693

[19] J. Morizur, M. Colla, and H. Bachor. (2008, Jul). Quantum noise detection: A portable and educational system. *American Journal of Physics*. [Online]. *76*(11). pp. 1022–1025. Available: https://doi-org.libproxy.nps.edu/10.1119/1.2969722

[20] C. M. Caves, "Quantum-mechanical noise in an interferometer," *Physical review. D, Particles and fields*, vol. 23, no. 8, pp. 1693–1708, Apr 1981. Available: https://doi-org.libproxy.nps.edu/10.1103/PhysRevD.23.1693

[21] M. Manicchia, "Construction and characterization of a dual atomic beam accelerometer/gyroscope," Ph.D. dissertation, Graduate School of Engineering and Applied Sciences, Naval Postgraduate School, Monterey, CA, June 2020. Available: https://calhoun.nps.edu/handle/10945/65398

[22] A. D. Cronin, J. Schmiedmayer, and D. E. Pritchard. (2009, Jul). Optics and interferometry with atoms and molecules. *Reviews of Modern Physics*. [Online]. *81*(3). pp.

1051–1129. Available: https://doi-org.libproxy.nps.edu/10.1103/RevModPhys.81.1051

[23] M. Kasevich and S. Chu, "Measurement of the gravitational acceleration of an atom with a light-pulse atom interferometer," *Applied Physics. B Photo-physics and Laser Chemistry*, vol. 54, pp. 321–332, Jan 1992. Available: https://link.aps.org/doi/10.1103/PhysRevLett.66.2689

[24] W. Demtröder, *Laser Spectroscopy 1 : Basic Principles*, 5th ed. Springer-Verlag Berlin Heidelberg, 2013.

[25] W. Heisenberg, "Über den anschaulichen inhalt der quantentheoretischen kinematik und mechanik," *Zeitschrift für Physik*, vol. 43, no. 3-4, pp. 172–199, Mar 1927. Available: https://doi.org/10.1007/BF01397280

[26] G. B. Rybicki, *Radiative Processes in Astrophysics*. New York: Wiley, 1979.

[27] S. T. Thornton, *Modern Physics for Scientists and Engineers*, 4th ed. Boston, MA: Brooks/Cole, 2013.

[28] Line Width and Line Shape. (n.d.). Technische Universität Braunschweig. [Online]. Available: http://www.pci.tu-bs.de/aggericke/PC4e/Kap_III/Linienbreite.htm. Accessed Oct. 30, 2020.

[29] M. Kaurav, *Engineering Chemistry with Laboratory Experiments*, 1st ed. Connaught Place, New Delhi, India: PHI Learning Private Limited, 2011.

[30] D. V. Schroeder, *An Introduction to Thermal Physics*, 1st ed. San Francisco, CA: Addison - Wesley, 1999.

[31] D. W. Preston, "Doppler-free saturated absorption: Laser spectroscopy," *American Journal of Physics*, vol. 64, no. 11, pp. 1432–1436, Nov 1996. Available: https://doi-org.libproxy.nps.edu/10.1119/1.18457

[32] P. Siddons, C. S. Adams, C. Ge, and I. G. Hughes, "Absolute absorption on rubidium d lines: comparison between theory and experiment," *Journal of Physics B: Atomic, Molecular and Optical Physics*, vol. 41, no. 15, pp. 155 004–, May 2008. Available: https://doi.org/doi:10.1088/0953-4075/41/15/155004

[33] A. Banerjee and V. Natarajan, "Saturated-absorption spectroscopy: eliminating crossover resonances by use of copropagating beams," *Optics letters*, vol. 28, no. 20, pp. 1912–1914, Oct 2003. Available: https://doi.org/10.1364/OL.28.001912

[34] *DLS1-A User's manual*, Teachspin, Inc., Buffalo, NY, 2011, rev 2.0 11/02.

[35] H. Rongqing and O. Maurice. (2009). *Fiber Optic Measurement Techniques*. Elsevier. Available: https://app.knovel.com/hotlink/toc/id:kpFOMT0001/fiber-optic-measurement/fiber-optic-measurement

[36] D. E. Jones, J. D. Franson, and T. B. Pittman, "Saturation of atomic transitions using subwavelength diameter tapered optical fibers in rubidium vapor," *Journal of the Optical Society of America B*, vol. 31, no. 8, pp. 1997–, Aug 2014. Available: https://doi.org/10.1364/JOSAB.31.001997

[37] P. A. M. Dirac, "The quantum theory of the emission and absorption of radiation," *Proceedings of the Royal Society of London. Series A, Containing Papers of a Mathematical and Physical Character*, vol. 114, no. 767, pp. 243–265, Mar 1927. Available: https://www.jstor.org/stable/94746

[38] R. J. Glauber, "Coherent and incoherent states of the radiation field," *Physical review*, vol. 131, no. 6, pp. 2766–2788, Sep 1963. Available: https://doi-org.libproxy.nps.edu/10.1103/PhysRev.131.2766

[39] V. M. et al., "Nep - noise equivalent power," Newton, NJ. Available: https://www.thorlabs.com/images/TabImages/Noise_Equivalent_Power_White_Paper.pdf

[40] D. Meschede, *Optics, Light and Lasers: The Practical Approach to Modern Aspects of Photonics and Laser Physics*, 2nd ed. WILEY-VCH, 2013.

[41] M. Kauranen, A. L. Gaeta, R. W. Boyd, and G. S. Agarwal, "Amplification of vacuum fluctuations by two-beam coupling in atomic vapors," *Physical Review A*, vol. 50, no. 2, pp. R929–R932, 1994. Available: https://doi-org.libproxy.nps.edu/10.1103/PhysRevA.50.R929

[42] W. Davis, M. Kauranen, E. Nagasako, R. Gehr, A. Gaeta, R. Boyd, and G. Agarwal, "Excess noise acquired by a laser beam after propagating through an atomic-potassium vapor," *Physical review. A, Atomic, molecular, and optical physics*, vol. 51, no. 5, pp. 4152–4159, May 1995. Available: https://doi-org.libproxy.nps.edu/10.1103/PhysRevA.51.4152

[43] B. G. Levi, "Squeezing the quantum noise limits," *Physics today*, vol. 39, no. 3, pp. 17–19, Mar 1986. Available: https://doi.org/10.1063/1.2814922

[44] D. Suter, *The Physics of Laser-Atom Interactions*, 2nd ed. Cambridge University Press, 2005.

[45] R. Loudon, *The Quantum Theory of Light*, 3rd ed. Great Clarendon Street, Oxford OX2 6DP: Oxford University Press, 2001.

[46] D. J. Griffiths, *Introduction to Electrodynamics*, 4th ed. Cambridge: Cambridge University Press, 2017.

[47] Q. Glorieux. (2015, Dec). Quantum Optics in Dense Atomic Media: From Optical Memories to Fluids of Light. Sciences Sorbonne Université - Laboratoire Kastler Brossel. [Online]. Available: https://www.researchgate.net/publication/329841768_Quantum_Optics_in_Dense_Atomic_Media_From_Optical_Memories_to_Fluids_of_Light

[48] N. Corzo, A. e. M. Marino, K. M. Jones, and P. D. Lett, "Multi-spatial-mode single-beam quadrature squeezed states of light from four-wave mixing in hot rubidium vapor," *Optics Express*, vol. 19, no. 22, pp. 21 358–21 369, Oct 2011. Available: https://doi.org/10.1364/OE.19.021358

[49] J. S. Bell, "On the einstein podolsky rosen paradox," *Physics Physique Fizika*, vol. 1, pp. 195–200, Nov 1964. Available: https://link.aps.org/doi/10.1103/PhysicsPhysiqueFizika.1.195

[50] Z. Peleg, R. Pnini, E. Yaarur, and E. Hecht, *Schaum's Outline of Quantum Mechanics*, 2nd ed. McGraw-Hill Professional Publishing, 2010.

[51] L. Mandel and E. Wolf, *Optical Coherence and Quantum Optics*, 1st ed. New York, NY: Cambridge University Press, 1995.

THIS PAGE INTENTIONALLY LEFT BLANK

Initial Distribution List

1. Defense Technical Information Center
   Ft. Belvoir, Virginia

2. Dudley Knox Library
   Naval Postgraduate School
   Monterey, California